

pubs.acs.org/JACS Article

How to Build Rigid Oxygen-Rich Tricyclic Heterocycles from Triketones and Hydrogen Peroxide: Control of Dynamic Covalent Chemistry with Inverse α -Effect

Ivan A. Yaremenko, Peter S. Radulov, Michael G. Medvedev, Nikolai V. Krivoshchapov, Yulia Yu. Belyakova, Alexander A. Korlyukov, Alexey I. Ilovaisky, Alexander O. Terent'ev,* and Igor V. Alabugin*



Cite This: J. Am. Chem. Soc. 2020, 142, 14588-14607



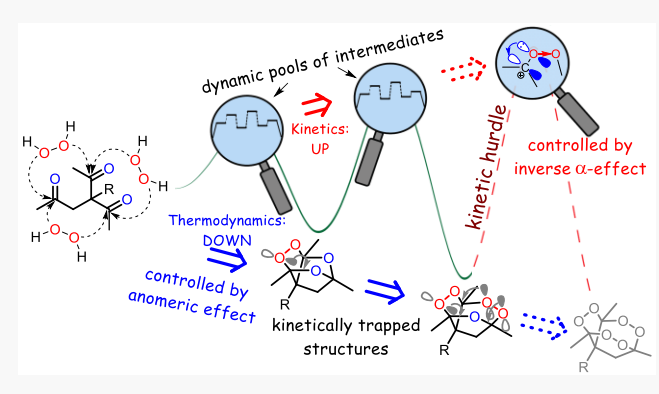
ACCESS

Metrics & More

Article Recommendations

Supporting Information

ABSTRACT: We describe an efficient one-pot procedure that "folds" acyclic triketones into structurally complex, pharmaceutically relevant tricyclic systems that combine high oxygen content with unusual stability. In particular, β , γ' -triketones are converted into three-dimensional polycyclic peroxides in the presence of H_2O_2 under acid catalysis. These transformations are fueled by stereoelectronic frustration of H_2O_2 , the parent peroxide, where the lone pairs of oxygen are not involved in strongly stabilizing orbital interactions. Computational analysis reveals how this frustration is relieved in the tricyclic peroxide products, where strongly stabilizing anomeric $n_O \rightarrow \sigma_{C-O}^*$ interactions are activated. The calculated potential energy surfaces for these transformations combine labile, dynamically formed cationic species with deply



stabilized intermediate structures that correspond to the introduction of one, two, or three peroxide moieties. Paradoxically, as the thermodynamic stability of the peroxide products increases along this reaction cascade, the kinetic barriers for their formation increase as well. This feature of the reaction potential energy surface, which allows separation of mono- and bis-peroxide tricyclic products, also explains why formation of the most stable tris-peroxide is the least kinetically viable and is not observed experimentally. Such unique behavior can be explained through the "inverse α -effect", a new stereoelectronic phenomenon with many conceptual implications for the development of organic functional group chemistry.

■ INTRODUCTION

Oxygen is one of the key elements of life. In addition to its many important biological functions (respiration, photosynthesis, biosynthesis), it plays an important role in photodynamic therapy, ¹ induction of apoptosis, etc. Importantly, oxygen is also one of the essential building components for the construction of both inorganic and organic molecules. Incorporation of oxygen, like a sprinkle of spice, adds many useful properties including polarity, H-bond formation, hydrophilicity, Lewis basicity, etc. to the plain hydrocarbon molecules. Not surprisingly, the functional groups that define undergraduate chemistry are mostly O-containing—from ethers and alcohols to ketones and carboxylic acid derivatives.

In this context, the relative obscurity of organic peroxides, a fundamentally important O-containing functionality, is both notable and unfortunate. Peroxides remain underutilized as structural components of organic molecules, despite offering a potentially very useful and conceptually different structural unit, i.e., the O-O bond, for molecular architecture.

Medicinal chemists recognize that peroxides offer a new mostly uncharted chemical space for drug development. Carbon and oxygen are near neighbors in the Periodic Table and the O—O and C—C bonds have important similarities: both bonds are nonpolar and the O—O distance in dimethyl peroxide (1.47 Å at the CCSD/cc-pVDZ level of theory) is only slightly shorter than the C—C distance of ethane (1.54 Å). However, peroxides are intrinsically more hydrophilic than alkanes due to the possibility of H-bond formation and the polarity of accompanying C—O bonds. Furthermore, the conformational profiles of C—C and O—O bonds are drastically different. Hence, introducing a peroxide in a chain or a cycle offers new means of perturbing polarities and molecular shapes, along with the ability to form H-

Received: June 10, 2020 Published: July 28, 2020





bonds—a useful combination of properties for modulation of supramolecular interactions and solubility.

The main challenge in using the O–O bond as a C–O/C–C bond isostere in drug design is that our ability to build three-dimensional peroxide-containing architectures is not as well-developed as our ability to make C–C bonds. And, of course, the greatest problem that plagues chemistry of peroxides is their perceived instability. To put it simply, peroxides have a bad reputation. Because of this reputation, the mere idea of using peroxides as a building block for making strained polycyclic structures similar to cubane, prismane, tetrahedrane, dodecahedrane, pagodane, and other architectural marvels of carbon chemistry may sound dangerous and perhaps even crazy, despite its esthetic appeal.

It is true that one has to approach peroxides carefully, but this bad reputation is not always fully justified. Electronic effects that lead to highly stable peroxides melting at >130 °C without decomposition² have been identified recently and shown to contribute to stability of artemisinin. Although chains made entirely from oxygens are unstable, the introduction of a single methylene unit in an $O-O-CH_2-O-O$ chain² or adding an acceptor group at the terminal oxygen atom³ significantly increases stability of peroxides.

Furthermore, one can argue that the C–C bonds (and the other strong bonds) do not have the monopoly as the structural elements for molecular construction. In this work, we will illustrate how the formation of complex cyclic structures can be achieved by taking advantage of the fact that the weaker bonds can be easily traded between molecules using mild dynamic covalent chemistry approaches.

The benefits from creating new polycyclic oxygen-rich systems are associated with the active development of new medicinal agents based on peroxides.⁴ In addition to serving as key chemical weapons against malaria (Figure 1),⁵ artemisinin,

Figure 1. Structures of natural, semisynthetic, and synthetic bioactive peroxides.

its derivatives, and analogues possess antiviral activity.⁶ Furthermore, polycyclic peroxides exhibit a broad spectrum of biological activities including high anthelmintic, ^{4e,7} antifungal, ⁸ anticancer, ⁹ and antitubercular properties. ¹⁰ The ethanolic extract of *Artemisia annua L*. is effective against SARS-associated coronavirus. ¹¹ Intriguingly, a recent report suggests that artemisinin is highly potent at inhibiting the ability of SARS-CoV-2 (the COVID-19 causing virus) to multiply while also having an excellent safety index. ¹²

The ability of carbonyl compounds and hydrogen peroxide to assemble into rigid three-dimensional polycyclic structures opens an efficient atom-economical synthetic path to cyclic peroxides like artemisinin. ¹³ The reaction of carbonyls with hydrogen peroxide is a black box that hides a surprising amount of complexity. Remarkably, this single type of peroxide-forming process opens access to various classes of peroxides, such as alkylperoxides, ¹⁴ geminal bis-peroxides, ¹⁵ 1,2-dioxolanes, ¹⁶ 1,2,4-trioxolanes, ^{8a,10a,17} 1,2,4-trioxanes, ¹⁸ 1,2,4,5-tetraoxanes, ¹⁹ and tricyclic monoperoxides. ²⁰

An intriguing feature of polycyclic peroxides is that they may bring us closer to "the peroxide island of stability". Although the instability of peroxides is notorious as illustrated, for example, by the highly explosive nature of triacetone triperoxide (TATP), 1 the origins of this instability can be complicated. For example, a thorough study of Keinan and co-workers concluded that, although the explosion of triacetone triperoxide (TATP) is not highly favored thermochemically, TATP is a powerful explosive due to "entropy explosion" associated with formation of multiple product molecules from every molecule of TATP. Note that such entropic burst would be greatly diminished for the polycyclic peroxides assembled from triketones.

The condensation of triketones can provide direct one-pot access to rigid tricyclic oxygen-rich structures from a flexible acyclic precursor. The rigidity of the structure is important for biological activity, because it decreases the entropic penalty for tight binding to the target.²³ Furthermore, it is also accompanied by significant increase in complexity due to the formation of the three new stereogenic centers and six new bonds.²⁴

However, the rich multifunctional nature of triketones also has a dark side derived from the unpredictable combination of multiple effects on reactivity. Potentially, the presence of three reaction centers can lead to the formation of a complex mixture of peroxides of various structures. In this regard, selective peroxidative cyclization of triketones is still an unsolved chemical challenge.

Our earlier work provided important corner pieces for solving this puzzle. In particular, we have shown previously how multiple peroxide moieties can stabilize each other and used this knowledge to control assembly of cyclic and bicyclic peroxides from ketones and diketones (Figure 2). 2,17c,d,25 For example, we have used a recently discovered stereoelectronic phenomenon, the inverse α -effect (vide infra), 25a to control the relative stabilities of oxacarbenium and peroxycarbenium ions formed from carbonyls and hydrogen peroxide under acid conditions to develop the first three-component couplings of ketoesters. 25b In parallel, we have applied stereoelectronic variations in anomeric $n_O \rightarrow \sigma_{C-O}^*$ interactions to selectively form either bis-peroxides or monoperoxides (ozonides) from diketones. 17c

Despite these advances, general rules are still lacking for the assembly of more complex polycyclic oxygen-rich systems, especially for the tricyclic systems. The literature includes only a few such systems prepared from tricarbonyl compounds. In particular, Rieche and co-workers prepared a tris-peroxide from triacetylmethane (the simplest $\beta_1 \hat{\beta}'$ -triketone) in 18% yield²⁶ and a bis-peroxide from triacetylethane (the simplest $\beta_{\gamma}\gamma'$ triketone) in 42% yield.²⁷ Despite the moderate yields, both of these reactions were quite selective and provided a single tricyclic ring system. Although the exclusive formation of trisperoxide from the $\beta_1\beta'$ -triketone could be explained by high strain of the alternative four-membered oxetane products, the observation of exclusive tricyclic bis-peroxide formation from the parent β, γ' -triketone did not have a simple explanation. Notably, these reactions were carried out under harsh conditions where H₂SO₄ was used as both a catalyst and a solvent (Figure

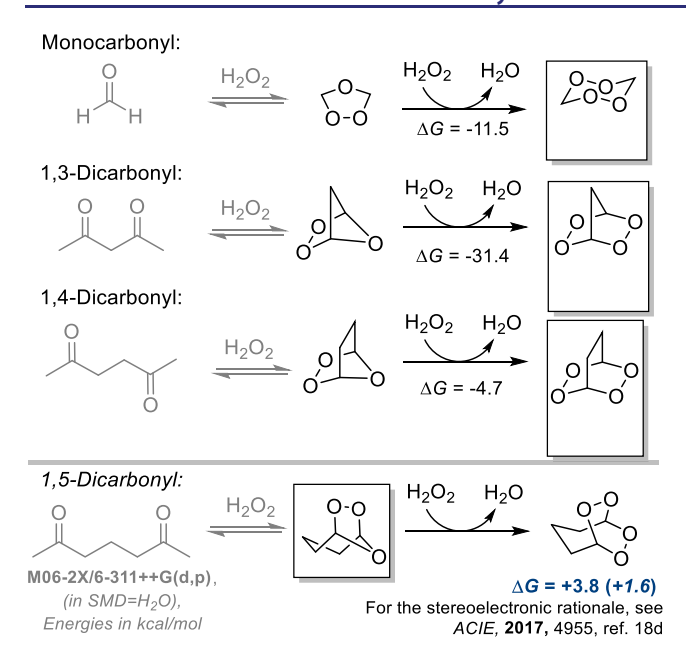


Figure 2. Tug-of-war in condensations of ketones and diketones can be controlled to provide either bis-peroxides or ozonides by selective deactivation of anomeric hyperconjugative interactions.

3). (It should be noted that many of these compounds can be extremely sensitive and explosive. In particular, the intermediary hydroperoxides that are formed as part of the product mixtures, can be much more explosive.) Furthermore, no successful synthesis of cyclic peroxides from other derivatives of triacetylmethane and triacetylethane was reported. Because of this scarcity, we were excited to discover that peroxidation of branched $\beta_1\delta'$ -triketones can proceed under milder condi-

tions.²⁸ We found that these reactions open access to three classes of tricyclic peroxides, namely tricyclic monoperoxides, bicyclic bis-peroxides (tetraoxanes), and bicyclic monoperoxides (ozonides). Although selective synthesis of one of these products (tricyclic monoperoxides) was developed, ^{20b-d} selective preparation of the other two peroxide families remained elusive, and no general rules have been suggested so far. Conspicuously, the longer the linker toward the third ketone group in the studied classes of triketones, the fewer peroxide moieties are incorporated in the final tricyclic product.

To make the situation even more interesting, Figure 3 provides thermodynamic driving forces for the observed bicyclic and tricyclic products. All of these cyclic products are more thermodynamically favorable than their acyclic precursors in the presence of hydrogen peroxide. However, it is clear that these cyclizations cannot be controlled solely by thermodynamics. Despite having a similar stability, tricyclic monoperoxides are formed selectively in the presence of strong Lewis acids while bicyclic bis-peroxides are not. Furthermore, the significantly less stable bicyclic monoperoxides (ozonides) are formed simultaneously with the much more stable alternative products under milder conditions.

These discoveries motivated us to revisit peroxidative condensations of β , γ' -triketones where, unlike β , β' -triketones, formation of both ether and peroxide bridges is possible. Our goal was to lay the foundation for the development of general guidelines that can describe the folding of multiple oxygencontaining chains into a complex rigid polycyclic structure. We also planned to explore if the stabilizing role of anomeric effect in peroxides was expanded to tricyclic structures and whether the thermodynamic driving force for incorporation of multiple peroxide units in a polycyclic core weakens when anomeric interactions are not fully activated. We also tested whether the

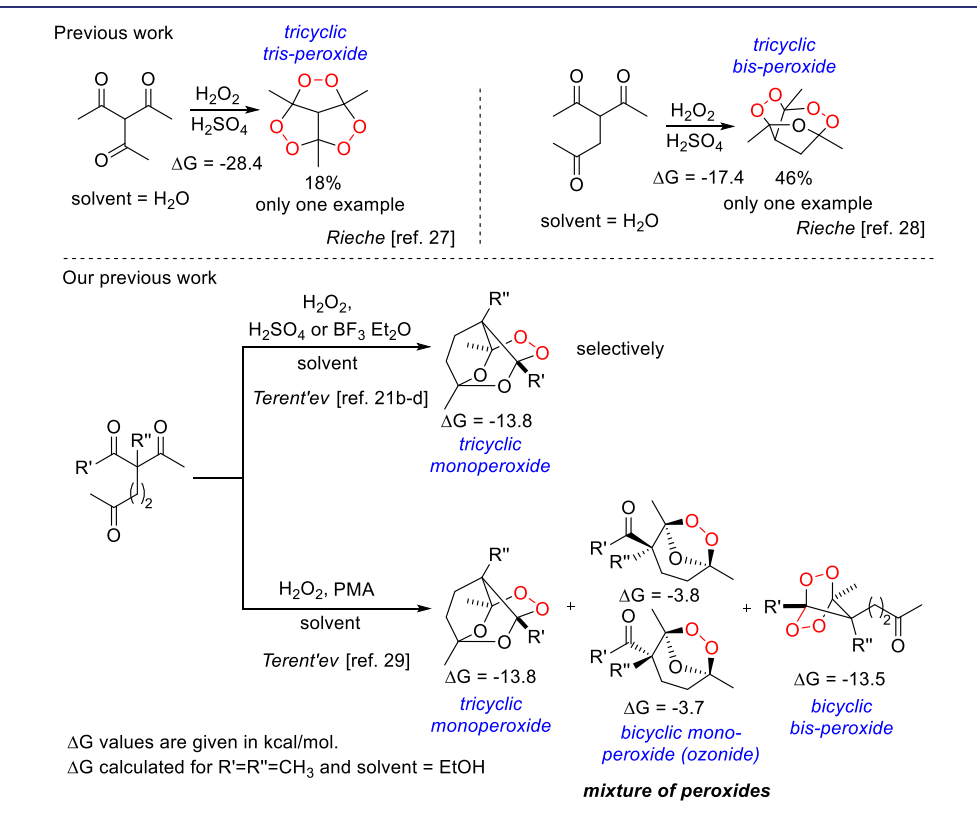


Figure 3. Examples of tricyclic oxygen-rich systems from triketones with calculated reaction Gibbs energies for their formation from the triketones.

Scheme 1. Synthesis of Tricyclic Monoperoxides 2l-q and Bis-peroxides 3a-p via Peroxidation of $\beta_i \gamma^i$ -Triketones 1a-q by H_2O_2

Scheme 2. General Thermodynamic Landscape for the Reaction of Triketone 1a with H₂O₂

OH
$$H_2O_2$$
 H_2O_2 H_2O_2

PBE0-D3BJ/6-311++G(d,p)/SMD(MeCN)

Energies in kcal/mol

peroxidative condensations of branched β , γ' -triketones and hydrogen peroxide proceed under kinetic control imposed by the recently discovered electronic effect, i.e., the inverse α -effect. From a practical point of view, we identified conditions where the formation of oxygen rich systems can stop after inclusion of either one or two O–O fragments and explain why the most thermodynamically stable tris-peroxide is not observed.

RESULTS AND DISCUSSION

Peroxidation of branched β , γ' -triketones 1a-q can be accomplished with aqueous or ethereal solution of hydrogen peroxide using BF₃·Et₂O, 98% H₂SO₄, 70% aq HClO₄, 50% aq HBF₄, or p-TsOH·H₂O. In the case of α -monosubstituted β , γ' -triketones 1a-k the reaction provided only tricyclic bisperoxides 3a-k. On the other hand, α -disubstituted β , γ' -triketones 1l-q can be used to assemble both tricyclic monoperoxides 2l-q and tricyclic bis-peroxides 3l-p (Scheme 1). The expected peroxides 4a-q with three O–O groups are not formed.

In order to gain an initial insight into the general thermodynamic landscape for this sequence of cyclizations, we calculated Gibbs free energy values for the formation of three tricyclic oxygen-rich systems (monoperoxide 2a, bis-peroxide **3a**, and tris-peroxide **4a**) from the parent β, γ' -triketone **1a** (Scheme 2).

The computational data show that each sequential conversion of an ether linkage into a peroxide linkage is favorable. Bisperoxide 3a is more stable than the monoperoxide 2a, whereas the tris-peroxide 4a is the most stable of these interconverting polycyclic species. Although the driving force for adding the last peroxide linkage is lower (\sim 2 kcal/mol) than for the introduction of the first and the second O–O units (\sim 7–8 kcal/mol), this increase in stability is still sufficiently large to expect that the tris-peroxide 4a would be favored under the full thermodynamic control.

In an attempt to find the optimal conditions for the assembly of oxygen rich systems from β , γ' -triketones, we studied the effect of nature and amount of the promoter (BF₃·Et₂O, 98% H₂SO₄, 70% aq HClO₄, 50% aq HBF₄, and p-TsOH·H₂O), reaction time, and variations in the nature of H₂O₂ (aqueous solution, ethereal solution) on the peroxidation of β , γ' -triketone 1a (Table 1).

The peroxidation of β , γ' -triketone 1a was initially carried out under anhydrous conditions. BF₃·Et₂O was used as a promoter while an ether solution of hydrogen peroxide was used as a reagent. Dry acetonitrile was used as a solvent since it dissolves all of the starting compounds, allowing the reaction mixture to

Table 1. Optimization Experiments for the Synthesis of Peroxide 3a from Triketone 1a and H₂O₂

	10	a	za, not formed	Sa	4a, not formed	
no.	acid (mol of acid/mol of 1a)	solvent	mol of $H_2O_2/mol 1a/type$ of H_2O_2	time (h)	NMR yield of 3a (%)	isolated yield of 3a (%)
1	BF ₃ ·Et ₂ O (0.5)	CH ₃ CN	3.0; 6.5 M ethereal	1	76	70
2	$BF_3 \cdot Et_2O$ (0.5)	CH ₃ CN	2.0; 6.5 M ethereal	1		53
3	BF ₃ ·Et ₂ O (0.25)	CH ₃ CN	3.0; 6.5 M ethereal	1		41
4	$BF_3 \cdot Et_2O$ (2.0)	CH ₃ CN	3.0; 6.5 M ethereal	1		47
5	$BF_3 \cdot Et_2O$ (0.5)	CH ₃ CN	3.0; 6.5 M ethereal	3		50
6	$BF_3 \cdot Et_2O$ (0.5)	CH ₃ CN	3.0; 6.5 M ethereal	0.5		69
7	$H_2SO_4(1.0)$	EtOH	3.0; 35% aq	1	traces	
8	$H_2SO_4(5.0)$	EtOH	3.0; 35% aq	1		17
9	$H_2SO_4(8.0)$	EtOH	3.0; 35% aq	1	34	20
10	$H_2SO_4(12.0)$	EtOH	3.0; 35% aq	1		40
11	$H_2SO_4(15.0)$	EtOH	3.0; 35% aq	1	71	60
12	$H_2SO_4(20.0)$	EtOH	3.0; 35% aq	1		28
13	$HClO_4(5.0)$	EtOH	3.0; 35% aq	1	20	
14	$HClO_4(10.0)$	EtOH	3.0; 35% aq	1	53	
15	$HClO_4(15.0)$	EtOH	3.0; 35% aq	1	64	63
16	$HClO_4(15.0)$	CH ₃ CN	3.0; 6.5 M ethereal	1	90	84
17	$HBF_4(10.0)$	EtOH	3.0; 35% aq	1	49	
18	$HBF_4(15.0)$	EtOH	3.0; 35% aq	1	80	77
19	$HBF_4(15.0)$	CH ₃ CN	3.0; 6.5 M ethereal	1	91	85
20	HBF ₄ (15.0)	CH ₃ CN	3.0; 35% aq	1	74	70
21	<i>p</i> -TsOH (0.5)	CH ₃ CN	3.0; 6.5 M ethereal	1	70	
22	<i>p</i> -TsOH (1.0)	CH ₃ CN	3.0; 6.5 M ethereal	1	90	
23	<i>p</i> -TsOH (2.0)	CH ₃ CN	3.0; 6.5 M ethereal	1	95	90
24	<i>p</i> -TsOH (2.0)	EtOH	3.0; 6.5 M ethereal	1	traces	

stay homogeneous. A typical procedure for peroxidation of $\beta_1\gamma'$ -triketone 1a was as follows: to a solution of the $\beta_1\gamma'$ -triketone 1a (0.300 g; 1.96 mmol) in MeCN (5 mL) at 20–25 °C was added H_2O_2 , followed by the promoter. The reaction mixture was then stirred at 20–25 °C. In the presence of substoichiometric (0.5 equiv) amounts of $BF_3 \cdot Et_2O$, the reaction of 3-fold molar excess of H_2O_2 in ether with triketone 1a led to a mixture of products containing the bis-peroxide 3a (70% isolated yield, expt 1). Neither the monoperoxide 2a nor, more surprisingly, the most thermodynamically favorable tris-peroxide 4a was observed.

Despite having the two peroxide bridges and the total of five oxygen atoms in the polycyclic frame (a half of atoms in the cyclic part), the tricyclic bis-peroxide 3a is a stable crystalline compound, which melts without decomposition at 119-121 °C. The 2D NMR correlation spectroscopic techniques (HSQC and HMBC) were used in analyzing the NMR spectra of the bisperoxides. For bis-peroxide 3a, the doublet at 3.28 ppm (CH) provides a characteristic ¹H NMR reference peak. Changes in the amount of BF3·Et2O slightly decrease the yields of bisperoxide 3a (exp. 3,4). The optimal reaction time was 1 h. Good results were achieved with several acids such as 98% H₂SO₄ in EtOH, and 70% aq HClO₄ or 50% aq HBF₄ in MeCN, where bis-peroxide 3a was obtained in 60%, 84%, and 85% isolated yields, respectively, when a 15-fold molar excess of acids was used (expts 11, 16, 19). A further increase in the amount of acid decreased the bis-peroxide yields.

Interestingly, an excellent result was obtained with p-TsOH· H_2O as promoter. In the presence of a 2-fold molar excess of p-TsOH· H_2O relative to triketone 1a, the bis-peroxide 3a was obtained in 90% isolated yield (expt 23). Furthermore, an increase in the amount of p-TsOH· H_2O to a 10-fold molar

excess of p-TsOH·H₂O relative to triketone **1a** did not lead to a decrease in the yield of bis-peroxide **3a**, in contrast to H₂SO₄, HClO₄, or HBF₄. Thus, the optimal conditions for the peroxidative condensation of triketone **1a** with H₂O₂ are the conditions for expt 23, in which 2-fold molar excess of p-TsOH·H₂O and 3-fold molar excess of 6.5 M solution of H₂O₂ in ether relative to triketone **1a** were used, and MeCN was used as solvent. Under these conditions, we can synthesize a variety of tricyclic bis-peroxides **3a**–k from triketones **1a**–k in good yields (Table 2).

Peroxidation of triketones 1a and 1b with small substituents near carbonyl groups proceeded with the formation of bisperoxides 3a, 3b in high yield (90% and 80%, respectively). In the case of bulky substituents, i.e., R^3 = isopropyl or cyclopropyl, the yield of bis-peroxides 3c and 3d was moderate -58% and 60%, respectively. Interesting results were obtained in the case of triketones 1e-g with aryl substituents near the γ' -carbonyl group. The oxygen-rich systems 3e-g turned out to be so stable that instead of an acid-catalyzed Hock²⁹/Udris-Sergeev³⁰-like rearrangement, we were able to obtain bis-peroxides 3e-g with an aryl group near the peroxide functionality in 37–45% yields. (The cumene process was described by Hock in 1944 and independently by Udris and Sergeev in 1942.) Remarkably, even bis-peroxides 3i-k with easily oxidized heterocycles, i.e., Nmethylindole and 2-methylfuran, at the bridged position were obtained in 35-48% isolated yields. Although the yield was low for bis-peroxide **3h** (only 14%), we found that the yield increases to 41% when a 5-fold molar excess of H₂O₂ was used instead of a 3-fold molar excess.

However, the reaction of a α -disubstituted β , γ' -triketone 11 formed two peroxides. Again the tris-peroxide formation was not

Table 2. Structures and Isolated Yields of Tricyclic Bis-peroxides 3a-k, Synthesized from Triketones 1a-ka

^aGeneral reaction conditions for Table 2: A 6.5 M ethereal solution of H_2O_2 (3.0 mol $H_2O_2/1.0$ mol 1a-k) and p-TsOH· H_2O (2.0 mol p-TsOH· $H_2O/1.0$ mol 1a-k) was successively added to a stirred solution of $\beta_1\gamma'$ -triketone 1a-k (0.300 g) in CH₃CN (10 mL) at 20–25 °C. The reaction mixture was stirred at 20–25 °C for 1 h. ^bFive-fold molar excess of 6.5 M solution of H_2O_2 in ether relative to triketone 1h was used.

Scheme 3. Peroxidation of Triketone 11

Table 3. Synthesis of Peroxides 2l and 3l from Triketone 1l and H₂O₂^a

"General reaction conditions for Table 3: A 6.5 M ethereal solution of H_2O_2 (1.0–5.0 mol of H_2O_2 /1.0 mol of 11) and p-TsOH (2.0 mol of p-TsOH/1.0 mol of 11) were successively added with stirring to a solution of $\beta_i \gamma'$ -triketone 11 (0.300 g, 1.76 mmol) in CH₃CN (5 mL) at 20–25 or –5 °C. The reaction mixture was stirred at 20–25 or –5 °C for 1 h.

Table 4. Structures and Isolated Yields of Tricyclic Monoperoxides 2l-q and Tricyclic Bis-peroxides 3l-p Synthesized from Triketones 1l-q

^aA 6.5 M ethereal solution of H_2O_2 (1.0 mol of $H_2O_2/1.0$ mol of 1l-q) and $p\text{-TsOH}\cdot H_2O$ (2.0 mol of $p\text{-TsOH}\cdot H_2O/1.0$ mol of 1l-q) were successively added to a stirred solution of β , γ' -triketone 1l-q (0.300 g) in CH₃CN (10 mL) at -5 °C. The reaction mixture was stirred at -5 °C for 1 h. ^bA 6.5 M ethereal solution of H_2O_2 (5.0 mol of $H_2O_2/1.0$ mol of 1l-q) and $p\text{-TsOH}\cdot H_2O$ (2.0 mol of $p\text{-TsOH}\cdot H_2O/1.0$ mol of 1l-q) were successively added to a stirred solution of β , γ' -triketone 1l-q (0.300 g) in CH₃CN (10 mL) at 20–25 °C. The reaction mixture was stirred at 20–25 °C for 1 h.

observed and a mixture of monoperoxide 2l and bis-peroxide 3l and was formed in 24% and 65% yields, respectively, by NMR (Scheme 3).

The structures of monoperoxide **2l** and bis-peroxide **3l** were unambiguously established by X-ray crystallographic analysis (Figure 5). For bis-peroxide **3l**, the characteristic ¹H NMR peaks of the CH₂ group show as the AB-system at 2.42 and 1.83 ppm for the two diastereotopic hydrogens. In contrast, the CH₂ group in monoperoxide **2l** is displayed as a characteristic singlet at 1.80 ppm. Monoperoxide **2l** and bis-peroxide **3l** are white crystalline compounds which melt without decomposition at 93–95 and 103–105 °C, respectively.

At the next step, we searched for optimal conditions for the selective transformation of α -disubstituted β , γ' -triketones in either monoperoxide or bis-peroxide using triketone 11 as model substrate (Table 3).

When the amount of hydrogen peroxide was lowered, the yield of the bis-peroxide 3l decreased from 65% to 5% while the yield of the monoperoxide 2l increased from 24% to 87% (expts 1–3, Table 3). The best yields for the monoperoxide 2l were achieved at -5 °C with 1 equiv of $\rm H_2O_2$ (93%, expt 4). In contrast, the 5-fold molar excess of hydrogen peroxide at the room temperature produced the bis-peroxide 3l in 95%. Remarkably, neither mono- nor tris-peroxide was observed under the latter conditions.

We have shown that the optimal conditions for the formation of monoperoxide 2l (expt 4) and for bis-peroxide 3l (expt 5) are general by extending them to the preparation of two parallel series of the tricyclic mono- and bis-peroxides. Each of these oxygen-rich systems was synthesized via the selective formation of three new cycles from acyclic α -disubstituted β , γ' -triketones 1l-q (Table 4).

Thus, substitution at the α -position of a β , γ' -triketone opened access to the first representatives of a new type of peroxides. These peroxides 2l-q were obtained in moderate (42% for 2p) to high (85% for 2l) isolated yields.

The size of the substituent at the α -position of $\beta_1 \gamma'$ -triketones adversely affects the yield of bis-peroxides 31-p. Thus, with an increase in the size of the substituent, the yield of bis-peroxides decreased from 87% for 31 to 30% for 3n. This situation can be explained by two factors. First, if the transition state for the bisperoxide formation is sensitive to the structure of the initial $\beta_1 \gamma'$ triketone, the insertion of an additional peroxide group may become a kinetically unfavorable process. The second factor may be an acid-catalyzed side-reaction of bis-peroxides 3m, 3n under the reaction conditions. This factor can contribute to the low yield of bis-peroxide 3o (20% vs 58% of bis-peroxide 3c). When peroxidation of triketone 10 with carried out with 5 equiv of H₂O₂, a complex mixture of products was formed. The characteristic peroxide ¹³C NMR signals in the 100–120 ppm region identified bis-peroxide 30 as the dominant peroxide component in this mixture that can be isolated in the individual form. On the other hand, the reaction of triketone 1q with a 5fold molar excess of hydrogen peroxide led to the respective monoperoxide 2q in good yield instead of the expected bisperoxide 3q.

In attempts to expand the scope of peroxidation of $\beta_1\gamma'$ -triketones, we investigated the possibility of converting monoperoxides to bis-peroxides and tris-peroxides. Indeed, the reaction of model monoperoxides 2l and 2n with 5-fold molar excess of hydrogen peroxide can transform them into bisperoxides 3l and 3n in 97% and 87% isolated yields, respectively (Scheme 4). However, further transformation of bis-peroxides 3a and 3l into tris-peroxides 4a and 4l was not observed.

All peroxygenated tricyclic products 3a-p and 2l-q were isolated in individual form by ordinary column chromatography on SiO_2 . 1H , ^{13}C NMR spectroscopy with using 2D correlation spectroscopic techniques can reliably distinguish 2 from 3. The structure of peroxides 2l, 3l, and 2q was unambiguously established by X-ray crystallographic analysis (Figure 4). All of these molecules are stable and melt at relatively high temperatures (2l: 93-95 °C; 3l: 103-105 °C; 2q: 190-191 °C).

Scheme 4. Peroxidation of Monoperoxides 2l,n and Bisperoxides 3a,l

■ COMPUTATIONAL ANALYSIS

All quantum-chemical calculations were performed with Gaussian 16^{31} program package at the PBE0 32 -D3BJ 33 /6-311+ +G(d,p) 34 /SMD 35 (MeCN) level of theory. PBE0 functional is known to provide accurate results for organic reactions 36 and has been recently shown to be well-grounded in theory. All computational results are based on quasiharmonically corrected free energies. Monte Carlo conformational search was performed for every computed intermediate and transition state. Numerical integration of kinetic equations was performed using the kinpy program. See the SI for further details.

Proposed Reaction Mechanism. As usual, multiple mechanistic scenarios exist for a multistep transformation. After analyzing a large number of possibilities (as summarized in the SI), we suggest the peroxidative condensation mechanism shown in Figure 5. The first step of the reaction is nucleophilic addition of H_2O_2 to a β -carbonyl group of triketone 1. The resulting intermediate I possess one nucleophilic (OOH) and two electrophilic (C=O) moieties. Reaction of the OOH group with one of the carbonyls yields the monocyclic endoperoxide II containing two exocyclic OH groups. Under the acidic conditions, the intermediate II transforms into bicyclic product III. Subsequent protonation of one of the exocyclic OH groups, followed by its elimination as water, leads to the formation of an oxacarbenium ion IV. Loss of water from a different position would lead to the formation of a less stable peroxycarbenium ion that is not shown here (see the SI). The key intermediate IV can either cyclize via the intramolecular capture of the cation by the remaining OH group to form the tricyclic monoperoxide product 2 or undergo a bimolecular reaction with an external H₂O₂ nucleophile to produce a bicyclic bis-peroxide V with the fused ether and peroxide rings. Elimination of a water molecule

from V leads to the formation of a peroxycarbenium ion VI (again expected to be less stable than a similar oxycarbenium ion due to the inverse α -effect). Intramolecular ring closure of this reactive cation results in the tricyclic bis-peroxide product 3. A number of other pathways were also considered but found to be less favorable (see the SI).

We have also investigated the mechanism of the tris-peroxide formation. The transformation begins with opening of the protonated ether cycle of 3. Depending on which of the two different C–O–C bonds is cleaved, the mechanism splits into two paths, proceeding through one of the isomeric peroxycarbenium ions, VII and X. The similar stability of these cation is (less than 1 kcal/mol difference for both R = H and Me) suggests that the magnitude of inverse α -effect in 5- and 6-membered peroxides is similar. Carbocations VII and X proceed on the path to the tricyclic tris-peroxide 4 via sequence of reactions that include nucleophilic addition of H_2O_2 and elimination of water. At this stage, one of the two new peroxycarbenium ions IX and XII is formed in the parallel pathways. Ring closures of either one of these ions provides the tricyclic tris-peroxide 4.

An interesting feature of this sequence is that formation of monoperoxide 2 avoids peroxycarbenium ions, formation of bisperoxide 3 goes through *one* peroxycarbenium ion, whereas formation of tris-peroxide 4 involves *two* more peroxycarbenium ions. Hence one would expect that properties of peroxycarbenium ions will gain progressively greater importance during this cascade transformation (vide infra).

Model Validation and Substituent Effects on Selectivity. We have validated this reaction model by comparing computational predictions with experimentally observed selectivity of peroxidation for four triketones summarized in Table 5.

As the first step, we have expanded our thermodynamic calculations to include the three substituted β , γ' -triketones 11,n,q (Figure 6). Several conclusions are immediately obvious. First, the formation of first tricyclic peroxide 21,n,q is much more favorable because the substituted substrates do not suffer the thermodynamic penalty for the enol–keto conversion in the reactant. Second, the larger groups decrease exergonicity for the tricyclic bis-peroxide formation by 2–4 kcal/mol in comparison to the conversion of their unsubstituted analogs $2a \rightarrow 3a$. Third, the similar decrease in stabilization is observed for the transformation of bis-peroxides to tris-peroxides, rendering the latter nearly thermoneutral or even mildly endergonic in some cases. Fourth, the calculated Gibbs free energies fail to reproduce the experimentally observed trends, suggesting that

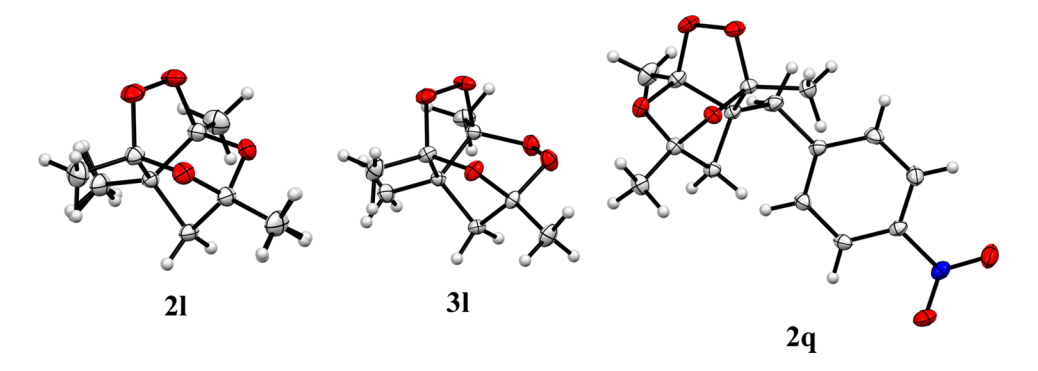


Figure 4. Molecular structures of 2l, 3l, and 2q. Atoms are presented as atomic displacement parameters (ADP) ellipsoids (50% probability).

Figure 5. Proposed mechanism of β , γ' -triketone 1 peroxidation.

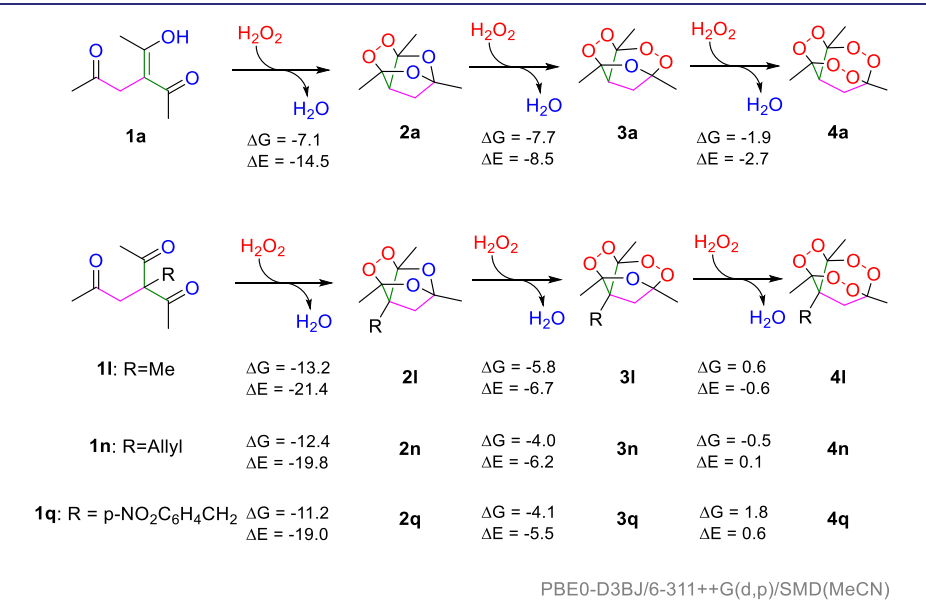
Table 5. Summary of Peroxidation Selectivity of Four Computationally Studied Substrates

	obsd products		
starting β , γ' -triketone	1 equiv of H ₂ O ₂	excess (5 equiv) of H ₂ O ₂	
1a, R = H	3a	3a	
11, R = Me	21	31	
1n, $R = Allyl$	2n	3n (slow)	
$\mathbf{1q}, R = p\text{-NO}_2C_6H_4CH_2$	2q	2q	

the assumption of thermodynamic control is not fully justified for these systems.

In particular, the free energy values suggest that the peroxidation of ${\bf 1a}$ and ${\bf 1q}$ with excess of ${\bf H_2O_2}$ should proceed up to tris-peroxide and bis-peroxide, correspondingly, while ${\bf 1l}$ and ${\bf 1n}$ should form mixtures of bis- and tris-peroxides under these conditions. These expectations completely disagree with the experiment. In particular, peroxidation of ${\bf 1l}$ and ${\bf 1n}$ with excess of ${\bf H_2O_2}$ terminates at bis-peroxides ${\bf 3l}$ and ${\bf 3n}$, while the reaction of ${\bf 1q}$ stops at the stage of monoperoxide ${\bf 2q}$. In the case of triketone ${\bf 1a}$, only traces of tris-peroxide ${\bf 4a}$ were detected even in the presence of a large excess (15 equiv) of ${\bf H_2O_2}$.

These discrepancies and results of control experiments (e.g., rates of $2a_il_in_iq \rightarrow 3a_il_in_iq$ reactions) suggest that kinetic factors control bis- and tris-peroxidations. Therefore, we have



Energies in kcal/mol

Figure 6. General thermodynamic landscape for the expanded selection of triketones with H_2O_2 . Note that introduction of substituent R adds a penalty for the formation of the second and third peroxide bridges.

computed free energies of intermediates and transition states on the paths from 2a,l,n,q to 3a,l,n,q and from 3a,l,n,q to 4a,l,n,q. To simplify the analysis, we will discuss bis- and tris-peroxide formation steps separately.

Kinetics of Bis-peroxide Formation. Figure 7 provides the full energy profile for the preferred path from the monoperoxide

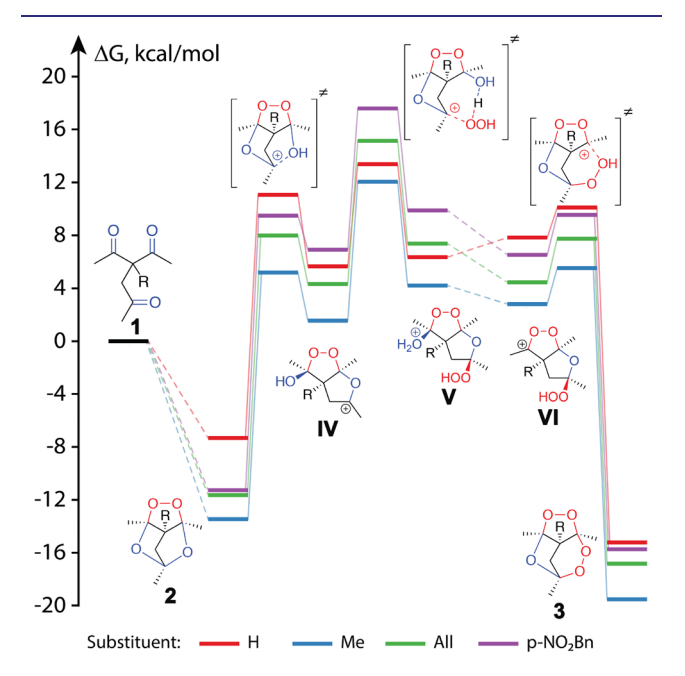


Figure 7. Potential energy surface of the peroxide-forming condensation cascade converting monoperoxides **2** to bis-peroxides **3**. Transition states and stationary points are joined by solid lines; pairs of stationary points are connected by dashed lines in cases where transition states of corresponding transformations were not located.

2 to the bis-peroxide 3 for four of the experimentally studied substituents. According to our results, the limiting step is the nucleophilic addition of H_2O_2 to the bicyclic oxacarbenium cations **IV**. The activation barriers were found to vary significantly depending on the substituent: from 20.7 to 29.0 kcal/mol.

Tris-peroxidation. Because analysis of the tris-peroxidation cascade is more complex, it will be given here only for substrates 1a and 11 (Figure 8). Similar to the bis-peroxidation stage, the limiting step for tris-peroxidation stage is the nucleophilic addition of H₂O₂ to a high energy bicyclic carbocation. However, unlike bis-peroxidation, the target carbocation reactant in the limiting step of tris-peroxidation is not an oxacarbenium ion but a peroxycarbenium ion. Remarkably, the calculated barriers for this step are much higher (33.0 to 36.2 kcal/mol) than for the analogous rate-limiting step in the bisperoxidation. Figure 8 illustrates that this dramatic barrier increase originates from two components: (a) reactant stabilization that stems from the high stability of bis-peroxide 3 and (b) transition state (TS) destabilization. The Hammond-Leffler postulate 40 connects the key transition states with the high energy peroxy-substituted cations such as X and XII, suggesting that the same electronic factor (the inverse α -effect, vide infra) is responsible for their destabilization.

Comparison of Experimental and Computed Selectivities. Trends in the calculated activation energies completely agree with the experimental observations. For example, bisperoxidation ($2a_il_in_iq \rightarrow 3a_il_in_iq$) tends to proceed slower in cases of larger substituents (see Table 5). Furthermore, trisperoxidation appears to be much more kinetically restricted than bis-peroxidation, so that only traces of tris-peroxide 4a could be detected experimentally.

Using the calculated free energy surfaces, we have modeled the evolution of this dynamic system by numerical integration of the kinetic equations (rate constants were computed from

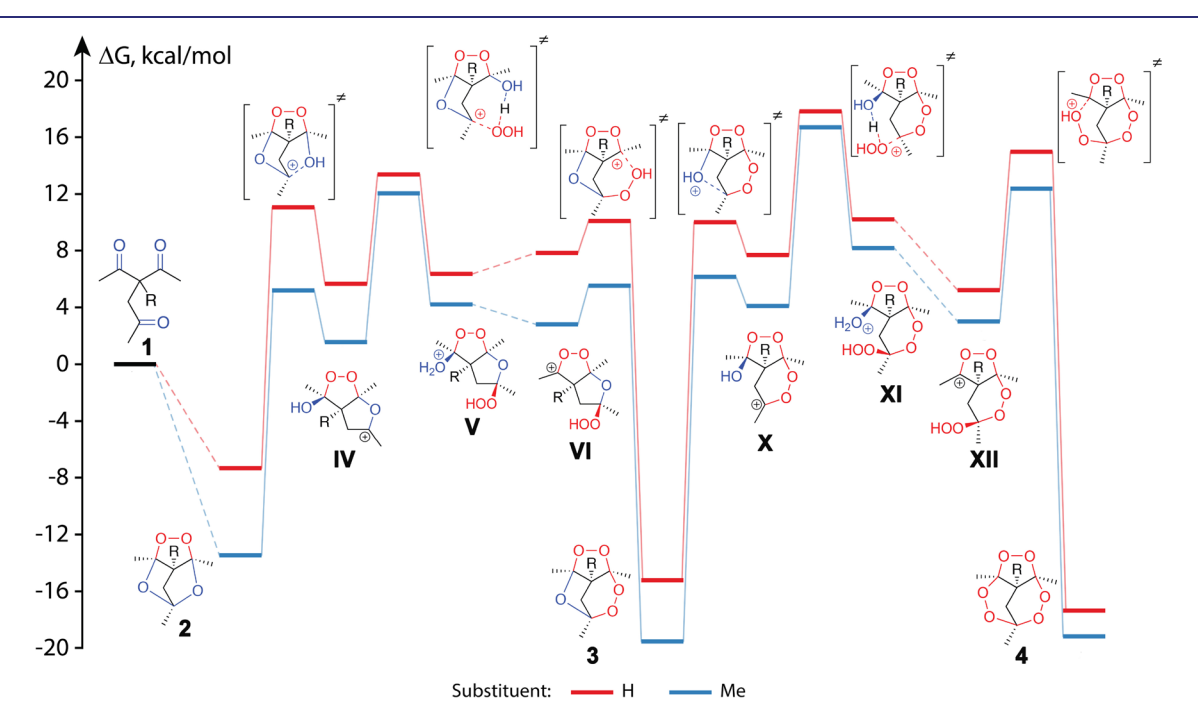


Figure 8. Potential energy surface of the full peroxide-forming condensation cascades. Transition states and stationary points are joined by solid lines; pairs of stationary points are connected by dashed lines in cases where transition states of corresponding transformations were not located. Calculations of triperoxidation stages were performed only for substrates 1a and 1l.

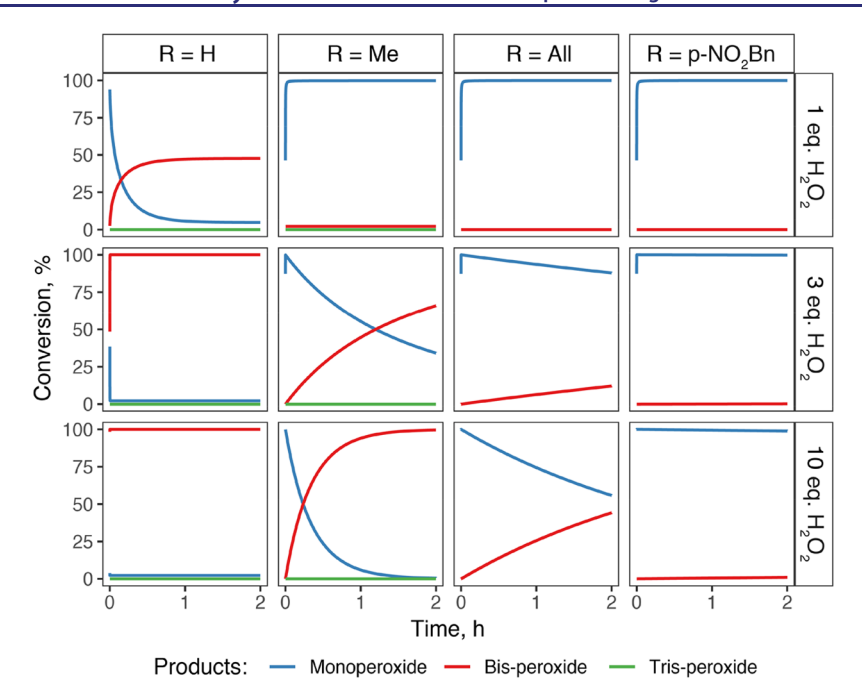


Figure 9. Concentration curves of 2-4 obtained for four different substrates and three levels of H_2O_2 concentration at the beginning. Calculations of tris-peroxidation stages were performed only for substrates 1a and 1l at 0 °C.

activation energies according to Eyring equation 41). Computed concentration curves (see Figure 9) show a significant decrease in transformation 1a,l,n, $q \rightarrow 3a$,l,n,q (3 equiv of H_2O_2) rate for substrates with larger substituents: 1a and 1l transform completely into bis-peroxide in 10 s and 1-2 h, respectively; 85% conversion of 1n to 3n (10 equiv of H_2O_2) is achieved in 6.5 h, while only 12% of 1q converts into 3q in 24 h in the presence of 10 equiv of H_2O_2 . Also, less than 0.01% yield of 4a,l,n,q (10 equiv of H_2O_2) in 100 h is expected according to the kinetic models. Thus, calculated activation free energy values agree with the experimental observations perfectly: reactions 2a, $l \rightarrow 3a$,l proceed freely, conversion $2n \rightarrow 3n$ is kinetically hindered, and whiletransformations $2q \rightarrow 3q$ and 3a, $l \rightarrow 4a$,l are blocked.

Stereoelectronic Model of Observed Reactivity and Selectivity. After succeeding in disentangling the mechanism of β , γ' -triketones peroxidation, our next goal was to identify the underlying theoretical concept which could be used to predict the outcome of similar reactions in the future. The central mystery of the entire scope of β , γ' -triketone peroxidation reactions is the extreme difficulty of tris-peroxidation, as opposed to, e.g., formation of triacetone triperoxide.

Kinetics and the Role of Inverse α -Effect. It is evident from Figure 8 that not only the transition states but also the peroxycarbenium cations on the path of tris-peroxidation are destabilized. Considering similar energies of these species, the Hammond–Leffler postulate suggests that they should have similar electronic and structural features as well. Similar carbocations with neighboring peroxide groups in a six-membered ring have been studied by us extensively and were shown to be strongly destabilized by the inverse α -effect. The essence of this new stereoelectronic effect is that a peroxide group provides much weaker carbocation stabilization in comparison to an ether group. This discovery goes against the expectation of greater donor ability of peroxide based on the classic α -effect, i.e., the enhancement of nucleophilicity due to the presence of an adjacent heteroatom in intermolecular

reactions. The fundamental question at the heart of both α -effects is whether the lone pairs of two directly connected heteroatoms can combine into a more powerful donor than each of the lone pairs taken separately. We found that contrary to the expectations based on the simple orbital mixing model, the lone pairs in a pair of directly connected heteroatoms are not raised in energy to become stronger donors toward adjacent acceptors. Instead, they are lowered by the inductive electron-withdrawing effect of the second oxygen atom of the peroxide.

In order to quantify the impact of inverse α -effect on destabilization of cation **X** and the consequent transition state, we considered isodesmic equations ^{25a} summarized in Figure 10. These equations allowed us to estimate the role of inverse α -effect in the activation energy of tris-peroxide formation for R = H and Me to be +17.2 and +17.4 kcal/mol. This penalty contributes significantly to the large activation barrier increases (by 12.3 and 10.7 kcal/mol) relative to the similar step in the bisperoxide formation (Figure 10).

An even more direct approach to computing the inverse α effect contribution to destabilization of carbocations and transition states is to evaluate the energies of orbital interactions in the key structures related to the rate-limited step of the cascade using Natural Bond Orbital (NBO) analysis. NBO is a very convenient approach for computational analysis of stereoelectronic interactions.⁴³ In order to do that, one has to force the NBO reference Lewis structure to change from the default oxarbenum $(-O^+=C-)$ description to the one where the oxygen retains both of its lone pairs and cationic carbon has an empty p-orbital. The absolute energies of $n_0 \rightarrow p^+$ interactions in Figure 11 should be taken as an approximation as these interactions are too strong for the second order perturbative estimate of orbital interactions to be accurate. However, the differences in the magnitude of such interactions are instructive: the cationic intermediate leading to the rate-limiting TS is destabilized by the inverse α -effect by \sim 14 kcal/mol whereas the TS loses about 11 kcal/mol of resonance stabilization for the same reason. These values agree well with the isodesmic

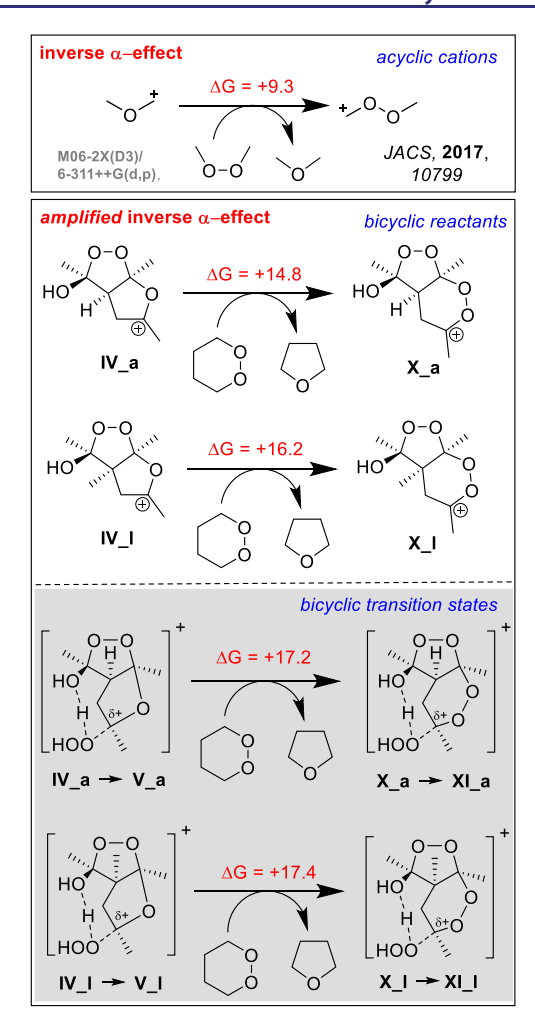


Figure 10. Isodesmic equations used to estimate destabilization of peroxycarbenium ions X_a and X_l and TSs of their reactions with hydrogen peroxide $(X_a, X_l \to XI_a, XI_l)$ imposed by inverse α -effect.

estimates given in Figure 10, even though the reference points for the comparisons are slightly different.

Thus, due to the inverse α -effect, any stage of peroxidation proceeding through nucleophilic addition to a peroxycarbenium ion suffers from a kinetic penalty. This penalty selectively blocked tris-peroxide formation from for all of the β , γ' -triketones explored in this work.

This conclusion is somewhat surprising because a similar well-known reaction of acetone with H_2O_2 proceeds exclusively to the tris-peroxide product. Notably, the main difference of this reaction from peroxidation of $\beta_i \gamma'$ -triketone is the absence of carbon bridges in the molecule. Indeed, it was recently shown that inverse α -effect becomes stronger when the peroxycarbenium ion is constrained in a five- or six-membered ring. This difference accounts for the experimentally significant increase in the activation barrier of tris-peroxidation. Indeed, the inverse α -effect at the rate-limiting TS connecting cations X and XI is \sim 8 kcal/mol stronger than in the parent acyclic cations (Figure 10).

We believe that the structural constraints imposed by the polycyclic frame make it impossible for the molecule to reach the optimal geometry for electronic stabilization. Therefore, the stereoelectronic penalty imposed by the additional linkages can amplify the role of the inverse α -effect in sequential peroxideforming condensations, potentially making incorporation of additional peroxide units into more rigid polycyclic systems more and more difficult (Figure 12).

Thermodynamics of Peroxidative Cascade Cyclizations: "Escape from Stereoelectronic Frustration" as the Driving Force for Inclusion of O–O Bridges in Polycyclic Structures. For these cascade transformation to proceed in high yields, thermodynamics for the condensation processes should be more favorable than for the reverse reaction (hydrolysis). In this context, an important question is why *is* the condensation with H_2O_2 favorable? What drives these transformations? These questions can be answered by analyzing the evolution of stereoelectronic effects in the O–O unit as it is transferred from hydrogen peroxide to the products of these cascade transformations.

There are two important clues to this puzzle, and both of them are stereoelectronic. In order to understand them, let us analyze the general thermodynamic landscape of the reaction of ketones with $\rm H_2O_2$. Figure 13 illustrates that this reaction is dramatically different from the analogous reaction with water. As is well

Figure 11. Direct comparison of $n_O \rightarrow p^+$ interactions in peroxycarbenium ions X and XIII (R = H) and transition states of their reactions with H_2O_2 . Because the strength of $n_O \rightarrow p^+$ interactions is influenced by the cycle size (see the SI), we have compensated for the difference in ring sizes by adding a CH₂ moiety in the reference oxycarbenium ion XIII and the respective TS.

Figure 12. Simplified reaction map for the cascade peroxidative cyclizations of the triketones highlighting the bicyclic peroxycarbenium and oxacarbenium ions.

M06-2X/6-311++G(d,p), Energies in kcal/mol

Figure 13. Contrasting thermodynamics for the reaction of acetone with H_2O and H_2O_2 .

known from an organic chemistry textbook, hydration of ketones with the formation of gem-diols is thermodynamically unfavorable. This is illustrated by the positive Gibbs free energy for the reaction of water with acetone (+6 kcal/mol at M06-2X/6-311++G(d,p) level 17c and +3 kcal/mol at the PBE0 level (SI)). In contrast, reaction of acetone with hydrogen peroxide is endergonic by only 1 kcal/mol. Furthermore, substitution of the remaining OH group in the mixed gem-OH/OOH species with the formation of bis-hydroperoxide is exergonic by \sim 4 kcal/mol. In other words, change of each OH group to an OOH group is exothermic by \sim 4–5 kcal/mol. Hence, the carbonyl group of the prototype ketone becomes reactive in the presence of H_2O_2 and engages in a reaction which "extracts" two molecules of H_2O_2 from the environment and attaches their peroxide moieties to the same

carbon. We will show below that this contrasting behavior is associated with "stereoelectronic frustration" of H_2O_2 .

Furthermore, this frustration is not fully relieved in the bishydroperoxide as evidenced by $-5.5 \, \text{kcal/mol}$ exothermicity of its reaction with acetone where one of the OOH groups is converted into an internal peroxide unit C-O-O-C (Figure 14). Since this species has both an OOH and an OH group, it can cyclize by losing either hydrogen peroxide or water. The first reaction forms a cyclic monoperoxide (ozonide) and is uphill by $+5 \, \text{kcal/mol}$, whereas the second reaction forms a cyclic bis-

$$\begin{array}{c} O \\ +2H_2O_2 \\ -H_2O \end{array} \begin{array}{c} HOO \\ OOH \\ AG = -5.5 \end{array} \begin{array}{c} OOH \\ OOH \\ -H_2O_2 \\ -H_2O_3 \end{array} \begin{array}{c} OOH \\ OOH \\ OOH \\ AG = -4.2 \end{array}$$

M06-2X/6-311++G(d,p), Energies in kcal/mol

Figure 14. Thermodynamic landscape for the reaction of acetone with *gem*-bis-hydroperoxides.

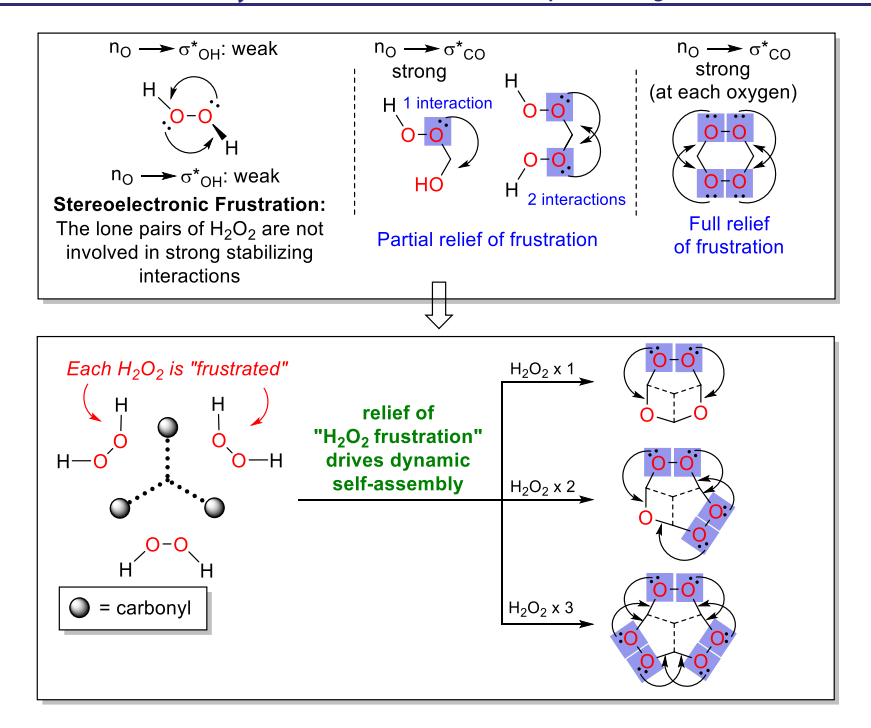


Figure 15. Concept of stereoelectronic frustration in H_2O_2 and frustration relief in organic hydroperoxides and peroxides.

peroxide and is downhill by -4 kcal/mol. Again, conversion of an OOH group to a cyclic peroxide is favorable whereas a similar conversion of an OH group into a cyclic ether is not.

Together these data clearly illustrate that reactions that consume H_2O_2 (and terminal -OOH moieties) are favorable whereas reactions that produce H_2O_2 are unfavorable. In other words, hydrogen peroxide is the high energy fuel that is consumed to form organic peroxides. So, what is different in hydrogen peroxide in comparison to organic peroxides?

We suggest that negative hyperconjugation, i.e., the stereoelectronic component of anomeric effect, as the main reason for these differences and that the anomeric interactions serve the key thermodynamic force assisting the assembly. The parent peroxide (hydrogen peroxide) is a high energy molecule due to the very limited opportunities for the frustrated peroxide lone pairs to engage in delocalizing hyperconjugative interactions (Figure 15).²

The stereoelectronic stabilization is switched on when two peroxides in the same molecule are separated by a single carbon atom (i.e., the peroxides are in a geminal arrangement). From this point of view, creation of the peroxide bridges is a way to remove a "frustrated" H_2O_2 molecule from solution and incorporate the O–O moiety in structure where each of the oxygen atoms has a suitable stereoelectronic partner in a stabilizing $n_O \rightarrow \sigma^*_{C-O}$ (anomeric) interaction.

In fact, even organic monoperoxides enjoy significant hyperconjugative stabilization via $n_O \rightarrow \sigma_{C-C}^*$ and $n_O \rightarrow \sigma_{C-H}^*$ interactions.⁴⁴ This stabilization increases in bis-peroxides where stronger $n_O \rightarrow \sigma_{C-O}^*$ interactions are present. This stereoelectronic force explains the greater stability of certain bis-peroxides in comparison to similar monoperoxides (Figure 16).

Our recent work revealed that the relative stability of bisperoxide and monoperoxide formed from bis-carbonyl systems is controlled by the bridge between the two ketone groups (Figure 17). While one-carbon and two carbon-bridges favor the formation of bis-peroxides, a three-carbon bridge renders

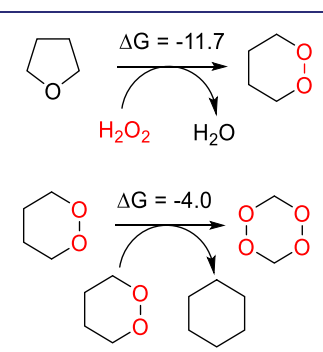


Figure 16. (Top) Hydrogen peroxide as high-energy fuel for creating organic peroxides. (Bottom) Combining two peroxides in one molecule provides additional stabilization by activating for anomeric $n_O \rightarrow \sigma_{C-O}^*$ interactions.

formation of monoperoxides (ozonides) more favorable than the formation of bis-peroxides. Interestingly, these trends in selectivity correlate with the magnitude of "anomeric" $^{17\rm d}$ $_{\rm O}\!\!\rightarrow\!\!\sigma_{\rm C-O}^*$ interactions in the bis-peroxide systems. The bis-peroxides (both monocyclic and bicyclic) were formed selectively in systems where these stabilizing hyperconjugative interactions are fully (or nearly fully) activated. However, in the case of 1,5-diketones, the expected bis-peroxide product has two of the four anomeric interactions nearly vanishing due to the geometric restraints of the twisted boat conformation of the bis-peroxide cycle.

Interestingly, this trend applies to the present formation of tricyclic systems derived from $\beta_{,\gamma}$ '-ketones. Only those peroxides are formed where the anomeric interactions are sufficiently strong. This condition is satisfied for the mono- and bis-peroxides but not in tris-peroxide (Figure 18).

The network of anomeric effects in the tricyclic systems is complex with six strong interactions of this type present. Importantly, in tris-peroxide, two of the 6 interactions are significantly weakened. Although this is a more subtle effect (average energies for mono-, bis- and tris-peroxides are 15.0,

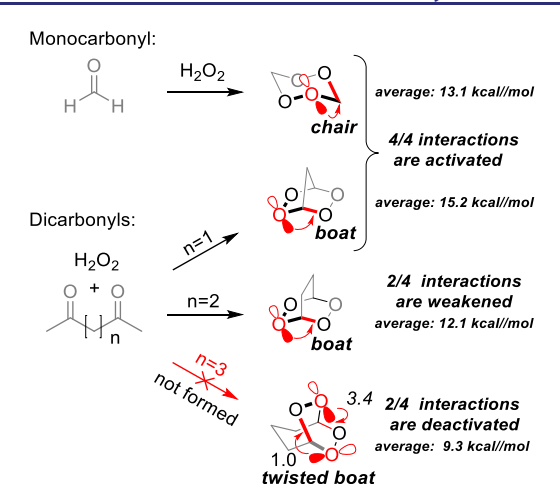


Figure 17. Deactivation of anomeric $n_O \rightarrow \sigma_{C-O}^*$ interactions by structural constraints can prevent formation of bis-peroxides in a bicyclic system. ^{17c} NBO energies for $n_O \rightarrow \sigma_{C-O}^*$ interactions shown by the arrows are calculated in kcal/mol at (SMD = MeCN)/B2PLYP-D2/6-311++G(d,p) level.

14.8, and 12.9 kcal/mol, respectively) than the one described above in Figure 17 for the bicyclic bis-peroxides, the difference clearly affects the balance by imposing a \sim 2 × 6 = 12 kcal/mol thermodynamic penalty for the tris-peroxide formation.

These results suggest a thermodynamic rule for the assembly of peroxide-rich cyclic, bicyclic and tricyclic structures that we formulate as follows: introduction of a new peroxide unit into a cycle is favored where all anomeric interactions with the available O-O units are activated.

CONCLUSION

The one-pot assembly of oxygen-rich systems, such as tricyclic mono- and bis-peroxides, was developed via reaction of β , γ' -triketones with H₂O₂, promoted such acids as BF₃·Et₂O, 98% H₂SO₄, 70% aq HClO₄, 50% aq HBF₄, p-TsOH·H₂O. Although the reaction of α -monosubstituted β , γ' -triketones leads to tricyclic bis-peroxides, the α -disubstituted β , γ' -triketones form both tricyclic bis-peroxides and tricyclic monoperoxides. The formation of monoperoxides or bis-peroxides from α -disubstituted β , γ' -triketones can be controlled by the relative excess of hydrogen peroxide and the reaction temperature. The thermodynamically favored tris-peroxides are not formed. The convenient feature of these reactions is that they are atom-efficient—water is the only byproduct.

Despite the very high oxygen content, the new peroxide-rich heterocycles are remarkably stable. For example, the tricyclic bisperoxide 3a, where five of the 10 atoms in the polycyclic framework are oxygens, is a white crystalline compound, which melts without decomposition at 119–121 °C despite having two peroxide bridges. Even more remarkably, the monoperoxide 2q starts to decompose only upon melting at 190 °C. Perhaps tricyclic peroxides are close to the "peroxide island of stability".

Several stereoelectronic conclusions emerge from the computational analysis. The combination of anomeric effect (product stabilization) and inverse α -effect (decreased positive charge stabilization in the TS and intermediate peroxycarbenium cations) puts each of the intermediate peroxides in a significantly deep potential energy well that allows it to be isolated if the right conditions exist. Indeed, we have identified reaction conditions that can stop at monoperoxidation or push the reaction toward bis-peroxidation.

We disentangle the mechanism of $\beta_i \gamma'$ -triketones peroxidation and show that inverse α -effect hinders reaction progress

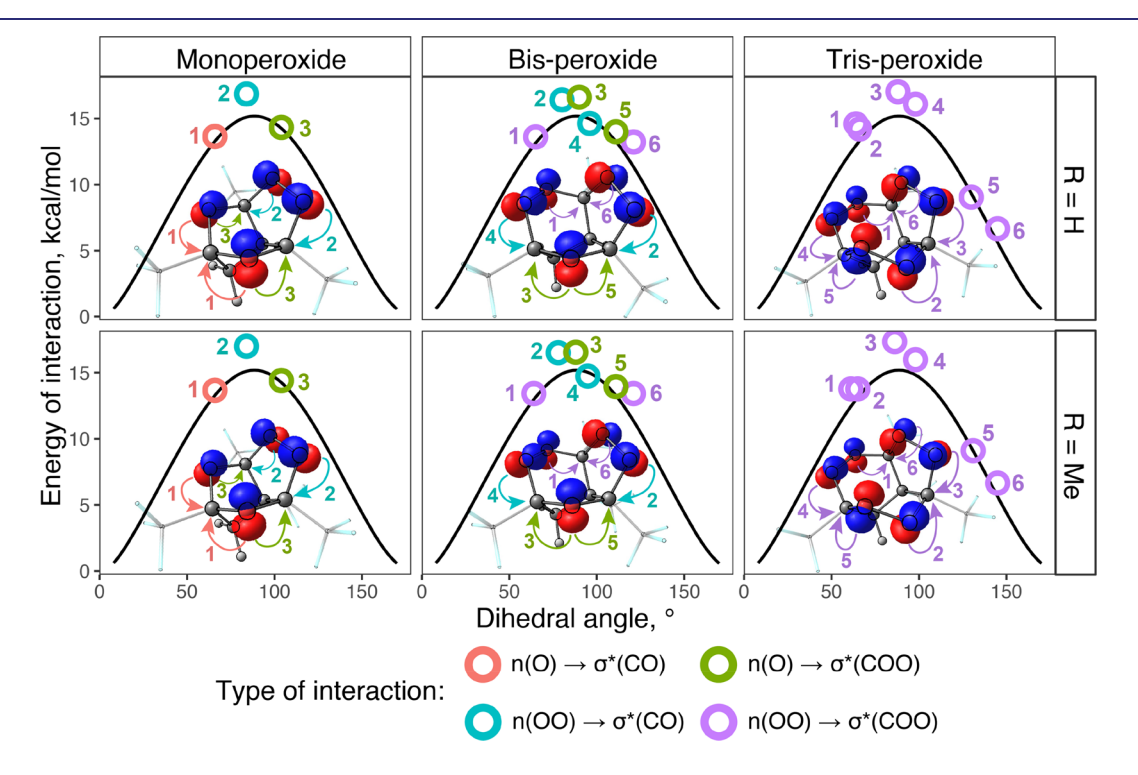


Figure 18. Networks of six $n_O \rightarrow \sigma_{C-O}^*$ interactions in each of the tricyclic mono-, bis-, and tris-peroxides derived from the parent and Me-substituted $\beta_i \gamma'$ -triketones. The black curves denote $n_O \rightarrow \sigma_{C-O}^*$ interaction energies for $CH_3 - O - CH_2 - O - CH_3$. Additional examples and extended analysis are given in the SI.

past bis-peroxides, so that tris-peroxides never form in measurable quantities. We also show that even though the reaction for four substituents (H, Me, All, p-NO₂Bn) proceeds through similar intermediates, the variability in relative energies of the intermediates and transition states makes the final reaction product depend heavily on the substituent. The calculated free energies are in complete agreement with the experimental results.

Under thermodynamic control, the main rule for the assembly of peroxide-rich cyclic, bicyclic and tricyclic structures is that introduction of a new peroxide unit into a cycle is favored where all anomeric interactions with the available O-O units are activated.

Despite the presence of many dynamically interconverting species connected by the multistep networks, peroxycondensations are not fully controlled by thermodynamics. A recently discovered stereoelectronic force, the inverse α -effect, introduces the key element of kinetic control by adding a penalty for the formation of both the peroxycarbenium ions and the transition states originating from these ions. This penalty can be amplified by the presence of acceptor groups or by geometric constraints.

Rules for assembling oxygen-rich systems from branched β, γ' triketones and hydrogen peroxide start to emerge. First, the introduction of each new peroxide ring to the tricyclic frameworks is progressively less exergonic. Second, in the case of α -disubstituted β , γ' -triketones, this cascade transformation can be conveniently stopped after the first peroxide bridge is formed, but it is also often possible to drive further to the formation of the second peroxide bridge. In the case of α monosubstituted $\beta_{,\gamma'}$ -triketones, the cascade transformation cannot be stopped after the formation of the first peroxide bridge. Third, the third peroxide bridge of the [5.2.2.0^{4,9}]tricyclic system is the most difficult to form. Even though this step is thermodynamically favorable, it is kinetically inhibited due to the combination of reactant stabilization (consequence of anomeric stabilization in peroxides) and lack of TS stabilization (consequence of inverse α -effect). Fourth, the peroxidation selectivity is determined by the size of the substituent R in the $\beta_i \gamma'$ -triketone: bis-peroxide is formed in case of unhindered R, while for larger R the selectivity shifts toward monoperoxide.

The tris-peroxidation remains elusive. It is completely averted by the inverse α -effect, showing the power of this recently discovered stereoelectronic phenomenon in controlling peroxidation processes. Once we can overcome this kinetic barrier, the formation of tris-peroxides will be possible.

ASSOCIATED CONTENT

Solution Supporting Information

The Supporting Information is available free of charge at https://pubs.acs.org/doi/10.1021/jacs.0c06294.

Experimental and additional computational details (PDF)
Calculations and jmol structure (XYZ)
X-ray data for compound 3l (CIF)
X-ray data for compound 2q (CIF)
X-ray data for compound 2l (CIF)

AUTHOR INFORMATION

Corresponding Authors

Alexander O. Terent'ev — N. D. Zelinsky Institute of Organic Chemistry, Russian Academy of Sciences, Moscow 119991, Russian Federation; ⊙ orcid.org/0000-0001-8018-031X; Email: terentev@ioc.ac.ru

Igor V. Alabugin — Department of Chemistry and Biochemistry, Florida State University, Tallahassee, Florida 32306, United States; ⊕ orcid.org/0000-0001-9289-3819; Email: alabugin@chem.fsu.edu

Authors

Ivan A. Yaremenko — N. D. Zelinsky Institute of Organic Chemistry, Russian Academy of Sciences, Moscow 119991, Russian Federation; © orcid.org/0000-0003-1068-9051

Peter S. Radulov — N. D. Zelinsky Institute of Organic Chemistry, Russian Academy of Sciences, Moscow 119991, Russian Federation

Michael G. Medvedev — N. D. Zelinsky Institute of Organic Chemistry, Russian Academy of Sciences, Moscow 119991, Russian Federation; ⊚ orcid.org/0000-0001-7070-4052

Nikolai V. Krivoshchapov — N. D. Zelinsky Institute of Organic Chemistry, Russian Academy of Sciences, Moscow 119991, Russian Federation; Lomonosov Moscow State University, Moscow 119991, Russia

Yulia Yu. Belyakova — N. D. Zelinsky Institute of Organic Chemistry, Russian Academy of Sciences, Moscow 119991, Russian Federation

Alexander A. Korlyukov — A. N. Nesmeyanov Institute of Organoelement Compounds, Russian Academy of Sciences, Moscow 119991, Russian Federation; orcid.org/0000-0002-5600-9886

Alexey I. Ilovaisky — N. D. Zelinsky Institute of Organic Chemistry, Russian Academy of Sciences, Moscow 119991, Russian Federation

Complete contact information is available at: https://pubs.acs.org/10.1021/jacs.0c06294

Notes

The authors declare no competing financial interest.

ACKNOWLEDGMENTS

A.O.T. and I.A.Y. are grateful for the support of the Russian Science Foundation (Grant No. 18-13-00027). I.V.A. is grateful for the support of the National Science Foundation (Grant No. CHE-1800329). Quantum chemical calculations were supported by Russian Science Foundation (Grant No. 19-13-00238). The Siberian Branch of the Russian Academy of Sciences (SB RAS) Siberian Supercomputer Center is gratefully acknowledged for providing supercomputer facilities. This work has been carried out using computing resources of the federal collective usage center Complex for Simulation and Data Processing for Mega-science Facilities at NRC "Kurchatov Institute", http://ckp.nrcki.ru/. The research was carried out using the equipment of the shared research facilities of HPC computing resources at Lomonosov Moscow State University.

REFERENCES

(1) (a) Juzeniene, A. Oxygen Effects in Photodynamic Therapy. In Handbook of Biophotonics; Popp, V. V., Tuchin, A. C., H, H. S., Eds.; Wiley, 2013; pp 305–313. (b) Hu, X.; Li, F.; Xia, F.; Guo, X.; Wang, N.; Liang, L.; Yang, B.; Fan, K.; Yan, X.; Ling, D. Biodegradation-Mediated Enzymatic Activity-Tunable Molybdenum Oxide Nanourchins for Tumor-Specific Cascade Catalytic Therapy. J. Am. Chem. Soc. 2020, 142 (3), 1636–1644. (c) Homma, T.; Kobayashi, S.; Fujii, J. Induction of ferroptosis by singlet oxygen generated from naphthalene endoperoxide. Biochem. Biophys. Res. Commun. 2019, 518 (3), 519–525. (d) Xuan, W.; Xia, Y.; Li, T.; Wang, L.; Liu, Y.; Tan, W. Molecular Self-Assembly of Bioorthogonal Aptamer-Prodrug Conjugate Micelles for Hydrogen Peroxide and pH-Independent Cancer Chemodynamic

Therapy. J. Am. Chem. Soc. 2020, 142 (2), 937–944. (e) Han, C.; Liu, Y.; Dai, R.; Ismail, N.; Su, W.; Li, B. Ferroptosis and Its Potential Role in Human Diseases. Front. Pharmacol. 2020, 11 (239), x. (f) Yang, W. S.; Stockwell, B. R. Ferroptosis: Death by Lipid Peroxidation. Trends Cell Biol. 2016, 26 (3), 165–176. (g) Murphy, M. P. Metabolic control of ferroptosis in cancer. Nat. Cell Biol. 2018, 20 (10), 1104–1105.

- (2) Gomes, G. d. P.; Vil', V. A.; Terent'ev, A. O.; Alabugin, I. V. Stereoelectronic source of the anomalous stability of bis-peroxides. *Chem. Sci.* **2015**, 6 (12), 6783–6791.
- (3) Reints, W.; Pratt, D. A.; Korth, H.-G.; Mulder, P. O-O Bond Dissociation Enthalpy in Di(trifluoromethyl) Peroxide (CF3OOCF3) as Determined by Very Low Pressure Pyrolysis. Density Functional Theory Computations on O-O and O-H Bonds in (Fluorinated) Derivatives. J. Phys. Chem. A 2000, 104 (46), 10713–10720.
- (4) (a) Nowak, D. M.; Lansbury, P. T. Synthesis of (+)-artemisinin and (+)-deoxoartemisinin from arteannuin B and arteannuic acid. Tetrahedron 1998, 54 (3), 319-336. (b) Stocks, P. A.; Bray, P. G.; Barton, V. E.; Al-Helal, M.; Jones, M.; Araujo, N. C.; Gibbons, P.; Ward, S. A.; Hughes, R. H.; Biagini, G. A.; Davies, J.; Amewu, R.; Mercer, A. E.; Ellis, G.; O'Neill, P. M. Evidence for a Common Non-Heme Chelatable-Iron-Dependent Activation Mechanism for Semisynthetic and Synthetic Endoperoxide Antimalarial Drugs. Angew. Chem., Int. Ed. 2007, 46 (33), 6278-6283. (c) Wang, X.; Zhao, Q.; Vargas, M.; Dong, Y.; Sriraghavan, K.; Keiser, J.; Vennerstrom, J. L. The activity of dispiro peroxides against Fasciola hepatica. Bioorg. Med. Chem. Lett. 2011, 21 (18), 5320-5323. (d) Coghi, P.; Yaremenko, I. A.; Prommana, P.; Radulov, P. S.; Syroeshkin, M. A.; Wu, Y. J.; Gao, J. Y.; Gordillo, F. M.; Mok, S.; Wong, V. K. W.; Uthaipibull, C.; Terent'ev, A. O. Novel Peroxides as Promising Anticancer Agents with Unexpected Depressed Antimalarial Activity (vol 13, pg 902, 2018). ChemMedChem 2018, 13 (20), 2249-2249. (e) Ingram, K.; Yaremenko, I. A.; Krylov, I. B.; Hofer, L.; Terent'ev, A. O.; Keiser, J. Identification of Antischistosomal Leads by Evaluating Bridged 1,2,4,5-Tetraoxanes, Alphaperoxides, and Tricyclic Monoperoxides. J. Med. Chem. 2012, 55 (20), 8700-8711. (f) Feng, Y.; Holte, D.; Zoller, J.; Umemiya, S.; Simke, L. R.; Baran, P. S. Total Synthesis of Verruculogen and Fumitremorgin A Enabled by Ligand-Controlled CH Borylation. J. Am. Chem. Soc. 2015, 137 (32), 10160-10163.
- (5) Rathi, A. Ranbaxy launches new anti-malarial Synriam. https://www.chemistryworld.com/news/ranbaxy-launches-new-anti-malarial-synriam/4967.article (accessed 08-10-2020).
- (6) (a) Efferth, T. Beyond malaria: The inhibition of viruses by artemisinin-type compounds. Biotechnol. Adv. 2018, 36 (6), 1730-1737. (b) D'Alessandro, S.; Scaccabarozzi, D.; Signorini, L.; Perego, F.; Ilboudo, D. P.; Ferrante, P.; Delbue, S. The Use of Antimalarial Drugs against Viral Infection. Microorganisms 2020, 8 (1), 85. (c) Efferth, T.; Romero, M. R.; Wolf, D. G.; Stamminger, T.; Marin, J. J. G.; Marschall, M. The Antiviral Activities of Artemisinin and Artesunate. Clin. Infect. Dis. 2008, 47 (6), 804-811. (d) Fröhlich, T.; Reiter, C.; Saeed, M. E. M.; Hutterer, C.; Hahn, F.; Leidenberger, M.; Friedrich, O.; Kappes, B.; Marschall, M.; Efferth, T.; Tsogoeva, S. B. Synthesis of Thymoquinone-Artemisinin Hybrids: New Potent Antileukemia, Antiviral, and Antimalarial Agents. ACS Med. Chem. Lett. 2018, 9 (6), 534-539. (e) Oiknine-Djian, E.; Weisblum, Y.; Panet, A.; Wong, H. N.; Haynes, R. K.; Wolf, D. G. The Artemisinin Derivative Artemisone Is a Potent Inhibitor of Human Cytomegalovirus Replication. Antimicrob. Agents Chemother. 2018, 62 (7), No. e00288. (f) Jacquet, C.; Marschall, M.; Andouard, D.; El Hamel, C.; Chianea, T.; Tsogoeva, S. B.; Hantz, S.; Alain, S. A highly potent trimeric derivative of artesunate shows promising treatment profiles in experimental models for congenital HCMV infection in vitro and ex vivo. Antiviral Res. 2020, 175, 104700. (g) Reiter, C.; Frohlich, T.; Gruber, L.; Hutterer, C.; Marschall, M.; Voigtlander, C.; Friedrich, O.; Kappes, B.; Efferth, T.; Tsogoeva, S. B. Highly potent artemisinin-derived dimers and trimers: Synthesis and evaluation of their antimalarial, antileukemia and antiviral activities. Bioorg. Med. Chem. 2015, 23 (17), 5452-5458.
- (7) (a) Cowan, N.; Yaremenko, I. A.; Krylov, I. B.; Terent'ev, A. O.; Keiser, J. Elucidation of the in vitro and in vivo activities of bridged 1,2,4-trioxolanes, bridged 1,2,4,5-tetraoxanes, tricyclic monoperoxides,

silyl peroxides, and hydroxylamine derivatives against Schistosoma mansoni. Bioorg. Med. Chem. 2015, 23 (16), 5175-5181. (b) Brecht, K.; Kirchhofer, C.; Bouitbir, J.; Trapani, F.; Keiser, J.; Krähenbühl, S. Exogenous Iron Increases Fasciocidal Activity and Hepatocellular Toxicity of the Synthetic Endoperoxides OZ78 and MT04. Int. J. Mol. Sci. 2019, 20 (19), 4880. (c) Wu, J.; Wang, X.; Chiu, F. C. K.; Häberli, C.; Shackleford, D. M.; Ryan, E.; Kamaraj, S.; Bulbule, V. J.; Wallick, A. I.; Dong, Y.; White, K. L.; Davis, P. H.; Charman, S. A.; Keiser, J.; Vennerstrom, J. L. Structure-Activity Relationship of Antischistosomal Ozonide Carboxylic Acids. J. Med. Chem. 2020, 63 (7), 3723-3736. (d) Fisher, L. C.; Blackie, M. A. Tetraoxanes as antimalarials: harnessing the endoperoxide. Mini-Rev. Med. Chem. 2014, 14, 123-135. (e) Ghorai, P.; Dussault, P. H.; Hu, C. Synthesis of spirobisperoxyketals. Org. Lett. 2008, 10, 2401-2404. (f) Hao, H. D.; Wittlin, S.; Wu, Y. Potent antimalarial 1,2,4-trioxanes through perhydrolysis of epoxides. Chem. - Eur. J. 2013, 19, 7605-7619. (g) Jefford, C. W. Synthetic Peroxides as Potent Antimalarials. News and Views. Curr. Top. Med. Chem. 2012, 12, 373-399. (h) Keiser, J.; Ingram, K.; Vargas, M.; Chollet, J.; Wang, X.; Dong, Y.; Vennerstrom, J. L. In vivo activity of aryl ozonides against Schistosoma species. Antimicrob. Agents Chemother. 2012, 56, 1090-1092. (i) Küster, T.; Kriegel, N.; Stadelmann, B.; Wang, X.; Dong, Y.; Vennerstrom, J. L.; Keiser, J.; Hemphill, A. Amino ozonides exhibit in vitro activity against Echinococcus multilocularis metacestodes. Int. J. Antimicrob. Agents **2014**, 43, 40–46. (j) Youyou Tu - Facts. *Nobel Media AB*2014, https:// www.nobelprize.org/prizes/medicine/2015/tu/facts/ (accessed 2020-08-10).2014 (k) Opsenica, D. M.; Šolaja, B. A. Antimalarial peroxides. J. Serb. Chem. Soc. 2009, 74, 1155-1193. (1) Šolaja, B. A.; Terzić, N.; Pocsfalvi, G.; Gerena, L.; Tinant, B.; Opsenica, D.; Milhous, W. K.; Fisher, L. C.; Blackie, M. A. Mixed steroidal 1,2,4,5-tetraoxanes: Antimalarial and antimycobacterial activity. J. Med. Chem. 2002, 45, 3331-3336. (m) Vil', V. A.; Yaremenko, I. A.; Ilovaisky, A. I.; Terent'ev, A. O. Peroxides with Anthelmintic, Antiprotozoal, Fungicidal and Antiviral Bioactivity: Properties, Synthesis and Reactions. Molecules 2017, 22 (11), 1881.

- (8) (a) Yaremenko, I. A.; Radulov, P. S.; Belyakova, Y. Y.; Demina, A. A.; Fomenkov, D. I.; Barsukov, D. V.; Subbotina, I. R.; Fleury, F.; Terent'ev, A. O. Catalyst development for the synthesis of ozonides and tetraoxanes under heterogeneous conditions. Disclosure of an unprecedented class of fungicides for agricultural application. *Chem. Eur. J.* 2020, 26, 4734–4751. (b) Yaremenko, I. A.; Syromyatnikov, M. Y.; Radulov, P. S.; Belyakova, Y. Y.; Fomenkov, D. I.; Popov, V. N.; Terent'ev, A. O. Cyclic Synthetic Peroxides Inhibit Growth of Entomopathogenic Fungus Ascosphaera apis without Toxic Effect on Bumblebees. *Molecules* 2020, 25 (8), 1954.
- (9) (a) Coghi, P.; Yaremenko, I. A.; Prommana, P.; Radulov, P. S.; Syroeshkin, M. A.; Wu, Y. J.; Gao, J. Y.; Gordillo, F. M.; Mok, S.; Wong, V. K. W.; Uthaipibull, C.; Terent'ev, A. O. Novel Peroxides as Promising Anticancer Agents with Unexpected Depressed Antimalarial Activity. ChemMedChem 2018, 13 (9), 902-908. (b) Yaremenko, I. A.; Coghi, P.; Prommana, P.; Qiu, C.; Radulov, P. S.; Qu, Y.; Belyakova, Y. Y.; Zanforlin, E.; Kokorekin, V. A.; Wu, Y. Y. J.; Fleury, F.; Uthaipibull, C.; Wong, V. K. W.; Terent'ev, A. O. Synthetic Peroxides Promote Apoptosis of Cancer Cells by Inhibiting P-Glycoprotein ABCB5. ChemMedChem 2020, 15 (13), 1118-1127. (c) Yaremenko, I. A.; Syroeshkin, M. A.; Levitsky, D. O.; Fleury, F.; Terent'ev, A. O. Cyclic peroxides as promising anticancer agents: in vitro cytotoxicity study of synthetic ozonides and tetraoxanes on human prostate cancer cell lines. Med. Chem. Res. 2017, 26 (1), 170-179. (d) Brautigam, M.; Teusch, N.; Schenk, T.; Sheikh, M.; Aricioglu, R. Z.; Borowski, S. H.; Neudorfl, J. M.; Baumann, U.; Griesbeck, A. G.; Pietsch, M. Selective Inhibitors of Glutathione Transferase P1 with Trioxane Structure as Anticancer Agents. ChemMedChem 2015, 10 (4), 629-639. (e) Abrams, R. P.; Carroll, W. L.; Woerpel, K. A. Five-Membered Ring Peroxide Selectively Initiates Ferroptosis in Cancer Cells. ACS Chem. Biol. 2016, 11, 1305-1312. (f) Chaudhari, M. B.; Moorthy, S.; Patil, S.; Bisht, G. S.; Mohamed, H.; Basu, S.; Gnanaprakasam, B. Iron-Catalyzed Batch/Continuous Flow C-H Functionalization Module for the Synthesis of Anticancer Peroxides. J. Org. Chem. 2018, 83 (3), 1358-

1368. (g) Dwivedi, A.; Mazumder, A.; du Plessis, L.; du Preez, J. L.; Haynes, R. K.; du Plessis, J. In vitro anti-cancer effects of artemisone nano-vesicular formulations on melanoma cells. *Nanomedicine* **2015**, *11* (8), 2041–2050.

(10) (a) Chaudhary, S.; Sharma, V.; Jaiswal, P. K.; Gaikwad, A. N.; Sinha, S. K.; Puri, S. K.; Sharon, A.; Maulik, P. R.; Chaturvedi, V. Stable Tricyclic Antitubercular Ozonides Derived from Artemisinin. *Org. Lett.* **2015**, *17*, 4948–4951. (b) Miller, M. J.; Walz, A. J.; Zhu, H.; Wu, C.; Moraski, G.; Möllmann, U.; Tristani, E. M.; Crumbliss, A. L.; Ferdig, M. T.; Checkley, L.; Edwards, R. L.; Boshoff, H. I. Design, Synthesis, and Study of a Mycobactin-Artemisinin Conjugate That Has Selective and Potent Activity against Tuberculosis and Malaria. *J. Am. Chem. Soc.* **2011**, *133* (7), 2076–2079. (c) Zhou, F. W.; Lei, H. S.; Fan, L.; Jiang, L.; Liu, J.; Peng, X. M.; Xu, X. R.; Chen, L.; Zhou, C. H.; Zou, Y. Y.; Liu, C. P.; He, Z. Q.; Yang, D. C. Design, synthesis, and biological evaluation of dihydroartemisinin- fluoroquinolone conjugates as a novel type of potential antitubercular agents. *Bioorg. Med. Chem. Lett.* **2014**, *24*, 1912–1917.

(11) (a) Yang, Y.; Islam, M. S.; Wang, J.; Li, Y.; Chen, X. Traditional Chinese Medicine in the Treatment of Patients Infected with 2019-New Coronavirus (SARS-CoV-2): A Review and Perspective. *Int. J. Biol. Sci.* 2020, 16 (10), 1708–1717. (b) Li, S.-y.; Chen, C.; Zhang, H.-q.; Guo, H.-y.; Wang, H.; Wang, L.; Zhang, X.; Hua, S.-n.; Yu, J.; Xiao, P.-g.; Li, R.-s.; Tan, X. Identification of natural compounds with antiviral activities against SARS-associated coronavirus. *Antiviral Res.* 2005, 67 (1), 18–23.

(12) Shah, A. Mateon Expands its COVID-19 Therapeutic Program to include Artemisinin. https://www.biospace.com/article/releases/mateon-expands-its-covid-19-therapeutic-program-to-include-artemisinin (accessed 2020-05-02).

(13) (a) Gilmore, K.; Kopetzki, D.; Lee, J. W.; Horváth, Z.; McQuade, D. T.; Seidel-Morgenstern, A.; Seeberger, P. H. Continuous synthesis of artemisinin-derived medicines. *Chem. Commun.* **2014**, *50* (84), 12652—12655. (b) Vil', V. A.; Yaremenko, I. A.; Ilovaisky, A. I.; Terent'ev, A. O. Synthetic Strategies for Peroxide Ring Construction in Artemisinin. *Molecules* **2017**, *22* (1), 117.

(14) (a) Terent'ev, A. O.; Borisov, D. A.; Yaremenko, I. A.; Chernyshev, V. V.; Nikishin, G. I. Synthesis of Asymmetric Peroxides: Transition Metal (Cu, Fe, Mn, Co) Catalyzed Peroxidation of β -Dicarbonyl Compounds with tert-Butyl Hydroperoxide. J. Org. Chem. 2010, 75 (15), 5065-5071. (b) Terent'ev, A. O.; Sharipov, M. Y.; Krylov, I. B.; Gaidarenko, D. V.; Nikishin, G. I. Manganese triacetate as an efficient catalyst for bisperoxidation of styrenes. Org. Biomol. Chem. 2015, 13 (5), 1439-1445. (c) Lan, Y.; Chang, X.-H.; Fan, P.; Shan, C.-C.; Liu, Z.-B.; Loh, T.-P.; Xu, Y.-H. Copper-Catalyzed Silylperoxidation Reaction of α,β -Unsaturated Ketones, Esters, Amides, and Conjugated Enynes. ACS Catal. 2017, 7 (10), 7120-7125. (d) Wang, H.; Chen, C.; Liu, W.; Zhu, Z. Difunctionalization of alkenes with iodine and tertbutyl hydroperoxide (TBHP) at room temperature for the synthesis of 1-(tert-butylperoxy)-2-iodoethanes. Beilstein J. Org. Chem. 2017, 13, 2023-2027. (e) Chaudhari, M. B.; Moorthy, S.; Patil, S.; Bisht, G. S.; Mohamed, H.; Basu, S.; Gnanaprakasam, B. Iron-Catalyzed Batch/ Continuous Flow C-H Functionalization Module for the Synthesis of Anticancer Peroxides. J. Org. Chem. 2018, 83 (3), 1358-1368. (f) Lu, S.; Tian, T.; Xu, R.; Li, Z. Fe- or co-catalyzed silylation-peroxidation of alkenes with hydrosilanes and T-hydro. Tetrahedron Lett. 2018, 59 (26), 2604-2606. (g) Xu, R.; Li, Z. Ag-catalyzed sulfonylationperoxidation of alkenes with sulfonyl hydrazides and T-hydro. Tetrahedron Lett. 2018, 59 (44), 3942-3945. (h) Yao, Y.; Wang, Z.; Wang, B. Tetra-n-butylammonium bromide (TBAB)-initiated carbonylation-peroxidation of styrene derivatives with aldehydes and hydroperoxides. Org. Chem. Front. 2018, 5 (16), 2501-2504. (i) Chaudhari, M. B.; Mohanta, N.; Pandey, A. M.; Vandana, M.; Karmodiya, K.; Gnanaprakasam, B. Peroxidation of 2-oxindole and barbituric acid derivatives under batch and continuous flow using an eco-friendly ethyl acetate solvent. React. Chem. Eng. 2019, 4 (7), 1277-1283. (j) Chen, Y.; Ma, Y.; Li, L.; Jiang, H.; Li, Z. Nitration-Peroxidation of Alkenes: A Selective Approach to β -Peroxyl Nitroalkanes. Org. Lett. 2019, 21 (5), 1480-1483.

(15) (a) Das, B.; Krishnaiah, M.; Veeranjaneyulu, B.; Ravikanth, B. A simple and efficient synthesis of gem-dihydroperoxides from ketones using aqueous hydrogen peroxide and catalytic ceric ammonium nitrate. Tetrahedron Lett. 2007, 48, 6286-6289. (b) Terent'ev, A. O.; Platonov, M. M.; Ogibin, Y. N.; Nikishin, G. I. Convenient Synthesis of Geminal Bishydroperoxides by the Reaction of Ketones with Hydrogen Peroxide. Synth. Commun. 2007, 37, 1281-1287. (c) Žmitek, K.; Zupan, M.; Stavber, S.; Iskra, J. The Effect of Iodine on the Peroxidation of Carbonyl Compounds. J. Org. Chem. 2007, 72, 6534-6540. (d) Ghorai, P.; Dussault, P. H. Mild and Efficient Re(VII)-Catalyzed Synthesis of 1,1-Dihydroperoxides. Org. Lett. 2008, 10, 4577-4579. (e) Terent'ev, A. O.; Platonov, M. M.; Krylov, I. B.; Chernyshev, V. V.; Nikishin, G. I. Synthesis of 1-hydroperoxy-1 '-alkoxyperoxides by the iodine-catalyzed reactions of geminal bishydroperoxides with acetals or enol ethers. Org. Biomol. Chem. 2008, 6 (23), 4435-4441. (f) Azarifar, D.; Khosravi, K.; Soleimanei, F. Stannous chloride dihydrate: A novel and efficient catalyst for the synthesis of gem-dihydroperoxides from ketones and aldehydes. Synthesis 2009, 2009, 2553-2556. (g) Li, Y.; Hao, H.-D.; Zhang, Q.; Wu, Y. A Broadly Applicable Mild Method for the Synthesis of gem-Diperoxides from Corresponding Ketones or 1,3-Dioxolanes. Org. Lett. 2009, 11, 1615-1618. (h) Kyasa, S.; Puffer, B. W.; Dussault, P. H. Synthesis of Alkyl Hydroperoxides via Alkylation of gem-Dihydroperoxides. J. Org. Chem. 2013, 78, 3452-3456. (i) Klussmann, M. Alkenyl and Aryl Peroxides. Chem. - Eur. J. 2018, 24 (18), 4480-4496.

(16) (a) Li, Y.; Wittlin, S.; Wu, Y. K. Antimalarial Spiro-Bridged 1,2-Dioxolanes Via Intramolecular Addition of Peroxycarbenium Ions to C-C Double Bonds. *Heterocycles* **2012**, *86* (1), 245–254. (b) Hurlocker, B.; Miner, M. R.; Woerpel, K. A. Synthesis of Silyl Monoperoxyketals by Regioselective Cobalt-Catalyzed Peroxidation of Silyl Enol Ethers: Application to the Synthesis of 1,2-Dioxolanes. Org. Lett. 2014, 16 (16), 4280-4283. (c) Kandur, W. V.; Richert, K. J.; Rieder, C. J.; Thomas, A. M.; Hu, C.; Ziller, J. W.; Woerpel, K. A. Synthesis and Reactivity of 1,2-Dioxolanes from β , γ -Epoxy Ketones. *Org. Lett.* **2014**, *16*, 2650–2653. (d) Zdvizhkov, A. T.; Terent'ev, A. O.; Radulov, P. S.; Novikov, R. A.; Tafeenko, V. A.; Chernyshev, V. V.; Ilovaisky, A. I.; Levitsky, D. O.; Fleury, F.; Nikishin, G. I. Transformation of 2-allyl-1,3-diketones to bicyclic compounds containing 1,2-dioxolane and tetrahydrofuran rings using the I-2/H2O2 system. Tetrahedron Lett. 2016, 57 (8), 949-952. (e) Xu, Z. J.; Wittlin, S.; Wu, Y. K. Probing the Peroxycarbenium [3 + 2] Cycloaddition Reactions with 1,2-Disubstituted Ethylenes: Results and Insights. Chem. - Eur. J. 2017, 23 (9), 2031-2034.

(17) (a) Griesbaum, K.; Liu, X.; Kassiaris, A.; Scherer, M. Ozonolyses of O-Alkylated Ketoximes in the Presence of Carbonyl Groups: A Facile Access to Ozonides. *Liebigs Ann.* 1997, 1997, 1381–1390. (b) Zvilichovsky, G.; Zvilichovsky, B. Ozonolysis. In *Hydroxyl, Ether and Peroxide Groups* (1993); John Wiley & Sons, Inc.: 2010; pp 687–784. (c) Yaremenko, I. A.; Gomes, G. d. P.; Radulov, P. S.; Belyakova, Y. Y.; Vilikotskiy, A. E.; Vil', V. A.; Korlyukov, A. A.; Nikishin, G. I.; Alabugin, I. V.; Terent'ev, A. O. Ozone-Free Synthesis of Ozonides: Assembling Bicyclic Structures from 1,5-Diketones and Hydrogen Peroxide. *J. Org. Chem.* 2018, 83 (8), 4402–4426. (d) Gomes, G. D.; Yaremenko, I. A.; Radulov, P. S.; Novikov, R. A.; Chernyshev, V. V.; Korlyukov, A. A.; Nikishin, G. I.; Alabugin, I. V.; Terent'ev, A. O. Stereoelectronic Control in the Ozone-Free Synthesis of Ozonides. *Angew. Chem., Int. Ed.* 2017, 56 (18), 4955–4959.

(18) (a) Griesbeck, A. G.; Brautigam, M.; Kleczka, M.; Raabe, A. Synthetic Approaches to Mono- and Bicyclic Perortho-Esters with a Central 1,2,4-Trioxane Ring as the Privileged Lead Structure in Antimalarial and Antitumor-Active Peroxides and Clarification of the Peroxide Relevance. *Molecules* 2017, 22 (1), 119. (b) Griesbeck, A. G.; Hoinck, L. O.; Lex, J.; Neudorfl, J.; Blunk, D.; El-Idreesy, T. T. 1,2,5,10,11,14-hexaoxadispiro[5,2.5.2]hexadecanes: Novel spirofused bis-trioxane peroxides. *Molecules* 2008, 13 (8), 1743–1758. (c) Rubush, D. M.; Morges, M. A.; Rose, B. J.; Thamm, D. H.; Rovis, T. An Asymmetric Synthesis of 1,2,4-Trioxane Anticancer Agents via Desymmetrization of Peroxyquinols through a Brønsted Acid Catalysis Cascade. *J. Am. Chem. Soc.* 2012, 134 (33), 13554–13557.

- (19) (a) Ghorai, P.; Dussault, P. H. Broadly Applicable Synthesis of 1,2,4,5-Tetraoxanes. Org. Lett. 2009, 11, 213-216. (b) Klapötke, T. M.; Stiasny, B.; Stierstorfer, J.; Winter, C. H. Energetic Organic Peroxides -Synthesis and Characterization of 1,4-Dimethyl-2,3,5,6tetraoxabicyclo[2.2.1]heptanes. Eur. J. Org. Chem. 2015, 2015, 6237-6242. (c) Novikov, V. L.; Shestak, O. P. Reactions of hydrogen peroxide with acetylacetone and 2-acetylcyclopentanone. Russ. Chem. Bull. 2013, 62, 2171-2190. (d) Terent'ev, A. O.; Borisov, D. A.; Chernyshev, V. V.; Nikishin, G. I. Facile and Selective Procedure for the Synthesis of Bridged 1,2,4,5-Tetraoxanes; Strong Acids As Cosolvents and Catalysts for Addition of Hydrogen Peroxide to β -Diketones. *J. Org. Chem.* **2009**, 74, 3335-3340. (e) Terent'ev, A. O.; Yaremenko, I. A.; Vil', V. A.; Moiseev, I. K.; Kon'kov, S. A.; Dembitsky, V. M.; Levitsky, D. O.; Nikishin, G. I. Phosphomolybdic and phosphotungstic acids as efficient catalysts for the synthesis of bridged 1,2,4,5-tetraoxanes from betadiketones and hydrogen peroxide. Org. Biomol. Chem. 2013, 11 (16), 2613-2623. (f) Yadav, N.; Sharma, C.; Awasthi, S. K. Diversification in the synthesis of antimalarial trioxane and tetraoxane analogs. RSC Adv. 2014, 4, 5469-5498.
- (20) (a) Eske, A.; Ecker, S.; Fendinger, C.; Goldfuss, B.; Jonen, M.; Lefarth, J.; Neudorfl, J. M.; Spilles, M.; Griesbeck, A. G. Spirofused and Annulated 1,2,4-Trioxepane-, 1,2,4-Trioxocane-, and 1,2,4-Trioxonane-Cyclohexadienones: Cyclic Peroxides with Unusual Ring Conformation Dynamics. *Angew. Chem., Int. Ed.* **2018**, *57* (42), 13770–13774. (b) Terent'ev, A. O.; Yaremenko, I. A.; Chernyshev, V. V.; Dembitsky, V. M.; Nikishin, G. I. Selective Synthesis of Cyclic Peroxides from Triketones and H2O2. *J. Org. Chem.* **2012**, *77*, 1833–1842. (c) Terent'ev, A. O.; Yaremenko, I. A.; Vil', V. A.; Dembitsky, V. M.; Nikishin, G. I. Boron Trifluoride as an Efficient Catalyst for the Selective Synthesis of Tricyclic Monoperoxides from beta, delta-Triketones and H2O2. *Synthesis* **2013**, *45* (2), 246–250. (d) Terent'ev, A. O.; Yaremenko, I. A.; Glinushkin, A. P.; Nikishin, G. I. Synthesis of peroxides from β , δ -triketones under heterogeneous conditions. *Russ. J. Org. Chem.* **2015**, *51*, 1681–1687.
- (21) Klapötke, T. M. Chemistry of High-Energy Materials, 3rd ed.; de Gruyter: Berlin, 2015.
- (22) Dubnikova, F.; Kosloff, R.; Almog, J.; Zeiri, Y.; Boese, R.; Itzhaky, H.; Alt, A.; Keinan, E. Decomposition of Triacetone Triperoxide Is an Entropic Explosion. *J. Am. Chem. Soc.* **2005**, *127* (4), 1146–1159.
- (23) Lawson, A. D. G.; MacCoss, M.; Heer, J. P. Importance of Rigidity in Designing Small Molecule Drugs To Tackle Protein-Protein Interactions (PPIs) through Stabilization of Desired Conformers. *J. Med. Chem.* **2018**, *61* (10), 4283–4289.
- (24) (a) Lovering, F.; Bikker, J.; Humblet, C. Escape from Flatland: Increasing Saturation as an Approach to Improving Clinical Success. *J. Med. Chem.* **2009**, *52* (21), *6*752–*6*756. (b) Cox, B.; Booker-Milburn, K. I.; Elliott, L. D.; Robertson-Ralph, M.; Zdorichenko, V. Escaping from Flatland: [2 + 2] Photocycloaddition; Conformationally Constrained sp3-rich Scaffolds for Lead Generation. *ACS Med. Chem. Lett.* **2019**, *10* (11), 1512–1517.
- (25) (a) Juaristi, E.; Gomes, G. D.; Terent'ev, A. O.; Notario, R.; Alabugin, I. V. Stereoelectronic Interactions as a Probe for the Existence of the Intramolecular alpha-Effect. J. Am. Chem. Soc. 2017, 139 (31), 10799-10813. (b) Vil, V. A.; Barsegyan, Y. A.; Barsukov, D. V.; Korlyukov, A. A.; Alabugin, I. V.; Terent'ev, A. O. Peroxycarbenium Ions as the "Gatekeepers" in Reaction Design: Assistance from Inverse Alpha-Effect in Three-Component beta-Alkoxy-beta-peroxylactones Synthesis. Chem. - Eur. J. 2019, 25 (63), 14460-14468. (c) Vil', V. A.; Gomes, G. D.; Bityukov, O. V.; Lyssenko, K. A.; Nikishin, G. I.; Alabugin, I. V.; Terent'ev, A. O. Interrupted Baeyer-Villiger Rearrangement: Building A Stereoelectronic Trap for the Criegee Intermediate. Angew. Chem., Int. Ed. 2018, 57 (13), 3372-3376. (d) Vil', V. A.; Barsegyan, Y. A.; Kuhn, L.; Ekimova, M. V.; Semenov, E. A.; Korlyukov, A. A.; Terent'ev, A. O.; Alabugin, I. V. Synthesis of unstrained Criegee intermediates: inverse α -effect and other protective stereoelectronic forces can stop Baeyer-Villiger rearrangement of γ-hydroperoxy-γperoxylactones. Chem. Sci. 2020, 11 (20), 5313-5322.

- (26) Rieche, A.; Bischoff, C.; Prescher, D. Alkylperoxyde, XXXV. Peroxyde des Triacetylmethans Triacetylmethanperoxyd. *Chem. Ber.* **1964**, 97 (11), 3071–3075.
- (27) Bischoff, C.; Rieche, A. Alkylperoxide, XXXVII1) Über die Bildung cyclischer Peroxide aus Mehrfachketonen. *Justus Liebigs Ann. Chem.* **1969**, 725 (1), 87–92.
- (28) Yaremenko, I. A.; Terent'ev, A. O.; Vil', V. A.; Novikov, R. A.; Chernyshev, V. V.; Tafeenko, V. A.; Levitsky, D. O.; Fleury, F.; Nikishin, G. I. Approach for the Preparation of Various Classes of Peroxides Based on the Reaction of Triketones with H2O2: First Examples of Ozonide Rearrangements. *Chem. Eur. J.* **2014**, *20* (32), 10160–10169.
- (29) Hock, H.; Lang, S. Autoxydation von Kohlenwasserstoffen, IX. Mitteil.: Über Peroxyde von Benzol-Derivaten. *Ber. Dtsch. Chem. Ges. B* **1944**, 77 (3–4), 257–264.
- (30) (a) Sergeyev, P. G.; Udris, R. J.; Kruzhalov, B. D.; Nyemtsov, B. D. Sposob odnovremennogo polucheniya fenola i acetona. USSR Patent 106992, 1947. (b) Udris, R. J.; Sergeyev, P. G.; Kruzhalov, B. D. Sposob polucheniya gidroperekisejj alkilirovannykh-proizvodnykh benzola ili alicikloaromaticheskikh uglevodorodov. USSR Patent 106666, 1947.
- (31) Frisch, M. J.; Trucks, G. W.; Schlegel, H. B.; Scuseria, G. E.; Robb, M. A.; Cheeseman, J. R.; Scalmani, G.; Barone, V.; Petersson, G. A.; Nakatsuji, H.; Li, X.; Caricato, M.; Marenich, A. V.; Bloino, J.; Janesko, B. G.; Gomperts, R.; Mennucci, B.; Hratchian, H. P.; Ortiz, J. V.; Izmaylov, A. F.; Sonnenberg, J. L.; Williams; Ding, F.; Lipparini, F.; Egidi, F.; Goings, J.; Peng, B.; Petrone, A.; Henderson, T.; Ranasinghe, D.; Zakrzewski, V. G.; Gao, J.; Rega, N.; Zheng, G.; Liang, W.; Hada, M.; Ehara, M.; Toyota, K.; Fukuda, R.; Hasegawa, J.; Ishida, M.; Nakajima, T.; Honda, Y.; Kitao, O.; Nakai, H.; Vreven, T.; Throssell, K.; Montgomery, J. A., Jr.; Peralta, J. E.; Ogliaro, F.; Bearpark, M. J.; Heyd, J. J.; Brothers, E. N.; Kudin, K. N.; Staroverov, V. N.; Keith, T. A.; Kobayashi, R.; Normand, J.; Raghavachari, K.; Rendell, A. P.; Burant, J. C.; Iyengar, S. S.; Tomasi, J.; Cossi, M.; Millam, J. M.; Klene, M.; Adamo, C.; Cammi, R.; Ochterski, J. W.; Martin, R. L.; Morokuma, K.; Farkas, O.; Foresman, J. B.; Fox, D. J. Gaussian 16, Rev. A.03; Wallingford, CT, 2016.
- (32) Adamo, C.; Barone, V. Toward reliable density functional methods without adjustable parameters: The PBE0 model. *J. Chem. Phys.* **1999**, *110* (13), 6158–6170.
- (33) Grimme, S.; Antony, J.; Ehrlich, S.; Krieg, H. A consistent and accurate ab initio parametrization of density functional dispersion correction (DFT-D) for the 94 elements H-Pu. *J. Chem. Phys.* **2010**, *132* (15), 154104.
- (34) (a) Krishnan, R.; Binkley, J. S.; Seeger, R.; Pople, J. A. Self-consistent molecular orbital methods. XX. A basis set for correlated wave functions. *J. Chem. Phys.* **1980**, 72 (1), 650–654. (b) Clark, T.; Chandrasekhar, J.; Spitznagel, G. W.; Schleyer, P. V. R. Efficient diffuse function-augmented basis sets for anion calculations. III. The 3-21+G basis set for first-row elements, Li–F. *J. Comput. Chem.* **1983**, 4 (3), 294–301.
- (35) Marenich, A. V.; Cramer, C. J.; Truhlar, D. G. Universal Solvation Model Based on Solute Electron Density and on a Continuum Model of the Solvent Defined by the Bulk Dielectric Constant and Atomic Surface Tensions. *J. Phys. Chem. B* **2009**, *113* (18), 6378–6396.
- (36) Mardirossian, N.; Head-Gordon, M. Thirty years of density functional theory in computational chemistry: an overview and extensive assessment of 200 density functionals. *Mol. Phys.* **2017**, *115* (19), 2315–2372.
- (37) (a) Medvedev, M. G.; Bushmarinov, I. S.; Sun, J. W.; Perdew, J. P.; Lyssenko, K. A. Density functional theory is straying from the path toward the exact functional. *Science* **2017**, 355 (6320), 49–52. (b) Mezei, P. D.; Csonka, G. I.; Kallay, M. Electron Density Errors and Density-Driven Exchange-Correlation Energy Errors in Approximate Density Functional Calculations. *J. Chem. Theory Comput.* **2017**, 13 (10), 4753–4764. (c) Marjewski, A. A.; Medvedev, M. G.; Gerasimov, I. S.; Panova, M. V.; Perdew, J. P.; Lyssenko, K. A.; Dmitrienko, A. O. Interplay between test sets and statistical procedures

- in ranking DFT methods: the case of electron density studies. *Mendeleev Commun.* **2018**, 28 (3), 225–235.
- (38) Grimme, S. Supramolecular Binding Thermodynamics by Dispersion-Corrected Density Functional Theory. *Chem. Eur. J.* **2012**, *18* (32), 9955–9964.
- (39) Srinivasan, A. Kinpy: A Source Code Generator for Solving Chemical Kinetic Equations in Python. https://code.google.com/archive/p/kinpy/ (accessed 08-10-2020).
- (40) (a) Leffler, J. E. Parameters for the Description of Transition States. Science 1953, 117 (3039), 340–341. (b) Hammond, G. S. A Correlation of Reaction Rates. J. Am. Chem. Soc. 1955, 77 (2), 334–338.
- (41) Evans, M. G.; Polanyi, M. Some applications of the transition state method to the calculation of reaction velocities, especially in solution. *Trans. Faraday Soc.* **1935**, *31* (0), 875–894.
- (42) (a) Edwards, J. O.; Pearson, R. G. The Factors Determining Nucleophilic Reactivities. *J. Am. Chem. Soc.* **1962**, 84 (1), 16–24. (b) Hoz, S.; Buncel, E. The α -Effect: A Critical Examination of the Phenomenon and Its Origin. *Isr. J. Chem.* **1985**, 26 (4), 313–319.
- (43) (a) Reed, A. E.; Weinhold, F. Natural localized molecular orbitals. *J. Chem. Phys.* **1985**, 83 (4), 1736–1740. (b) Reed, A. E.; Curtiss, L. A.; Weinhold, F. Intermolecular interactions from a natural bond orbital, donor-acceptor viewpoint. *Chem. Rev.* **1988**, 88 (6), 899–926. (c) Weinhold, F. *Encyclopedia of Computational Chemistry*, 3rd ed.; Wiley, 1998; p 1972. (d) Weinhold, F.; Landis, C. R.; Glendening, E. D. What is NBO analysis and how is it useful? *Int. Rev. Phys. Chem.* **2016**, 35 (3), 399–440. (e) Gomes, G. d. P.; Alabugin, I. V. Stereoelectronic Effects: Analysis by Computational and Theoretical Methods, *Applied Theoretical Organic Chemistry*; World Scientific, 2018; pp 451502.
- (44) Alabugin, I. V. Stereoelectronic Effects: the Bridge between Structure and Reactivity; John Wiley & Sons Ltd.: Chichester, UK, 2016.
- (45) Sadovnichy, V.; Tikhonravov, A.; Voevodin, V.; Opanasenko, V. Lomonosov: Supercomputing at Moscow state university. *Contemp. High perform. Comput. From petascale toward exascale*; CRC Press: Boca Raton, 2013.